CALIFORNIA STATE UNIVERSITY, NORTHIDGE

Shear Wave Velocity Structure and Evolution of Old Oceanic Lithosphere: Constraints from Rayleigh Wave Dispersion across a Local Array of Ocean-Bottom Seismometers

A thesis submitted in partial fulfillment of the requirements for the degree of Masters of Science in Geophysics

By
Lexine Black

December 2015

The thesis of Lexine Black is approved by:

_____	_____
Gerry Simila, Ph.D.	Date
_____	_____
Matthew d'Alessio, Ph.D.	Date
_____	_____
Dayanthie Weeraratne, Ph. D., Chair	Date

California State University Northridge

Table of Contents

List of Figures

List of Equations

ABSTRACT

Shear Wave Velocity Structure and Evolution of Old Oceanic Lithosphere: Constraints from Rayleigh Wave Dispersion across a Local Array of Ocean-Bottom Seismometers

By

Lexine Black

Masters of Science in Geophysics

Although plate tectonic theory was first proposed in the early 1900's, the very nature and process of tectonic plate formation is actively debated today, with arguments for simple conductive cooling and growth with advancing seafloor age versus arguments presented for the influence of mantle dynamic sources. Could the plate tectonic system and mantle convection cycle be linked via buoyance forces and flow in the asthenosphere, which catalyze plate formation and growth? Seafloor subsidence values for ages less than 80 Ma are satisfied by the half-space conductive cooling model, but these parameters deviate from the linearly described model for older seafloor. There is a paucity of data from old seafloor to address this discrepancy. I investigate the lithospheric structure of a section of 150-160 Ma seafloor in the northwestern Pacific using Rayleigh wave phase velocity data. My results indicate high velocities of 4.7 km/s $\pm$ 0.07 km/s in the upper lithosphere that extend to ~65 km depth. I observe a negative velocity gradient with a minimum of 4.30 $\pm$ 0.09 km/s at 150 km depth. The lithosphere-asthenosphere boundary, defined by the negative velocity gradient below the high velocity lid, occurs at 90 km $\pm$ 35 km. The highest velocities in my study region are higher than previous studies of 5-9 Ma seafloor, but similar to studies of 100 Ma seafloor. High velocities in the 150 Ma seafloor I studied are similar to velocities typically observed in the upper lithosphere of Archean cratons. This similarity suggests that continental evolution is a complex process of multi-layered growth whereas the evolution of oceanic lithosphere is a simple, single layer process of growth. Half space cooling may be sufficient to explain

the evolution process but alternative models of interaction with dynamic mantle sources cannot be ruled out.

CHAPTER 1
Introduction

1.1 Motivation

Since the discovery and acceptance of plate tectonics in the mid 1900's, the movement and age of plates have been well measured, but we still know very little about the physical properties of plates and what mantle properties facilitate plate movement. The prohibitive access to oceanic lithosphere in deep water has limited research to use of land instrumentation with teleseismic raypaths which sample the seafloor. The physical properties of the lithosphere, its physical dimensions, and the cause of the sharp boundary at its base is actively debated. Authors have explained the lithosphere's physical properties by conductive cooling (Parsons and Sclater, 1977; McKenzie and Pristley, 2005), the natural increase in pressure and temperature in the Earth (Stixrude and Lithgow-Bertelloni, 2005), dehydration (Evans et al., 2006), grain size effects (Faul and Jackson, 2005), or a permeable dehydration boundary (Rychert et al., 2011). Each of these properties will have different effects on seismic wave propagation. Thickness and mass of plates control many aspects of the plate tectonic system including the seafloor depth, subsidence rate, cooling rate of the Earth's interior (Parsons and Sclater, 1977), speed of internal convection (Richter and Parsons, 1975), and style of subduction and arc volcanism. (Nyblade, 2002). Here I analyze seismic wave velocities collected by the marine seismic PLATE (Pacific Lithosphere Anisotropy Thickness Experiment) projectconducted in the northwest Pacific in old seafloor with age of 150-160 Ma. I seek to identify seismic velocities in this unique region of oceanic plates to constrain some of the physical properties and processes debated above for oceanic lithosphere formation.

1.2 Background

The boundary between lithosphere and asthenosphere (LAB) is defined as a dramatic contrast in viscosity. The depth at which this transition can be inferred from petrologic (Priestly and McKenzie 2006) and seismic methods (Booth et al., 2014; Gaherty et al., 1999). Evidence from two different techniques using seismic waves show that LAB is a particularly sharp boundary (Gaherty et al.,1999; Rychert et al., 2006).

What gives rise to this change in mechanical properties and why does it occur at the depth that it does? Studies have proposed that the LAB is

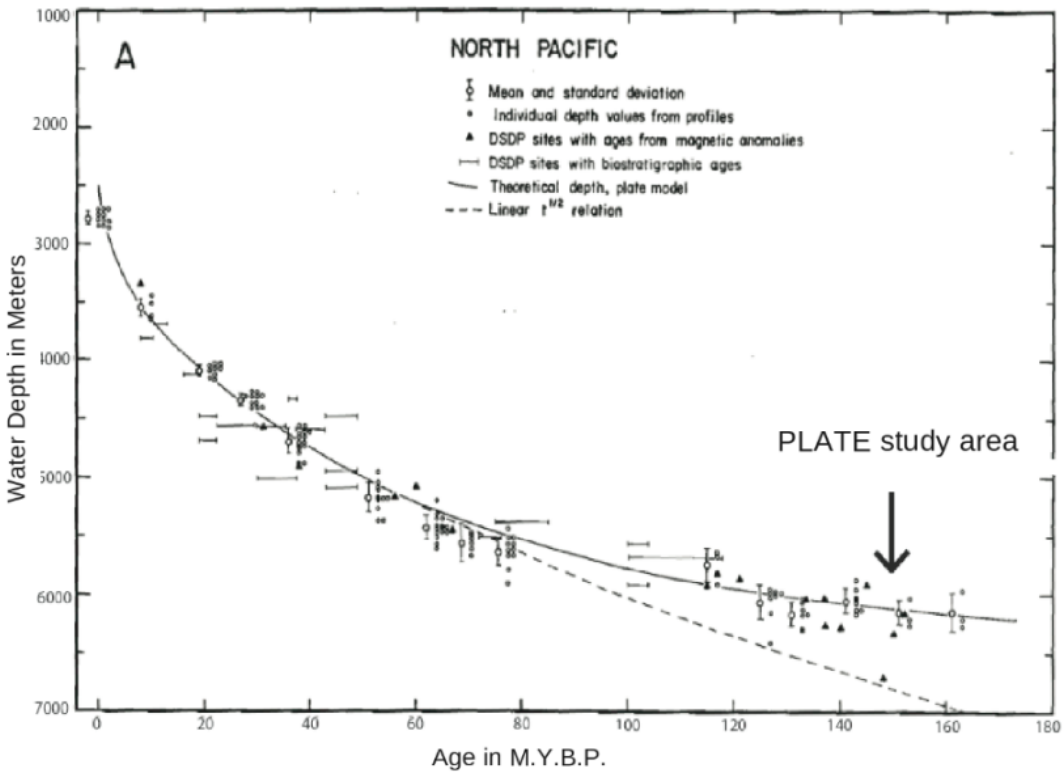

Figure 1. Seafloor depths as a function of age (Parsons and Sclater, 1977). Circles and triangles represent bathymetry measurements from the Pacific ocean. Dashed line represents the half- space cooling model, solid line represents the Plate model.

best modeled as a thermal transition (e.g. Ritzwoller et al. 2004), compositional boundary (Jordan, 1978), or phase change (Walter et al., 1998), among other suggestions. .

To better constrain this transition, observations of other well constrained properties such as density, crustal thickness, and cooling rate are used to approximate plate thickness, which is defined by the LAB. Currently, the best form of seafloor data are heat flux and water depth. Heat flux and water depth measurements are compared with theoretical models (Figure 1) for age dependence (Parsons and Sclater, 1977). The conductive cooling model accurately predicts the observed seafloor depth and heat flow magnitude for seafloor up to 80 Ma; for older crust, the model overestimates observed subsidence and heat flow. Bathymetry shows water depth reaches an asymptotic value at old ages, raising the question of what mechanism is responsible for this behavior. .

However, limitations in the mere availability of data in sufficiently old seafloor, as well as sparse studies or restricted use only land seismic stations with paths that travel across ocean basins, raise the importance of these simple questions. Here, I will present the results of shear wave inversions of Rayleigh wave phase velocity data collected from the PLATE project. The PLATE project was conducted in the northwest Pacific to study the discrepancy between predicted and observed subsidence data shown in Figure 2.

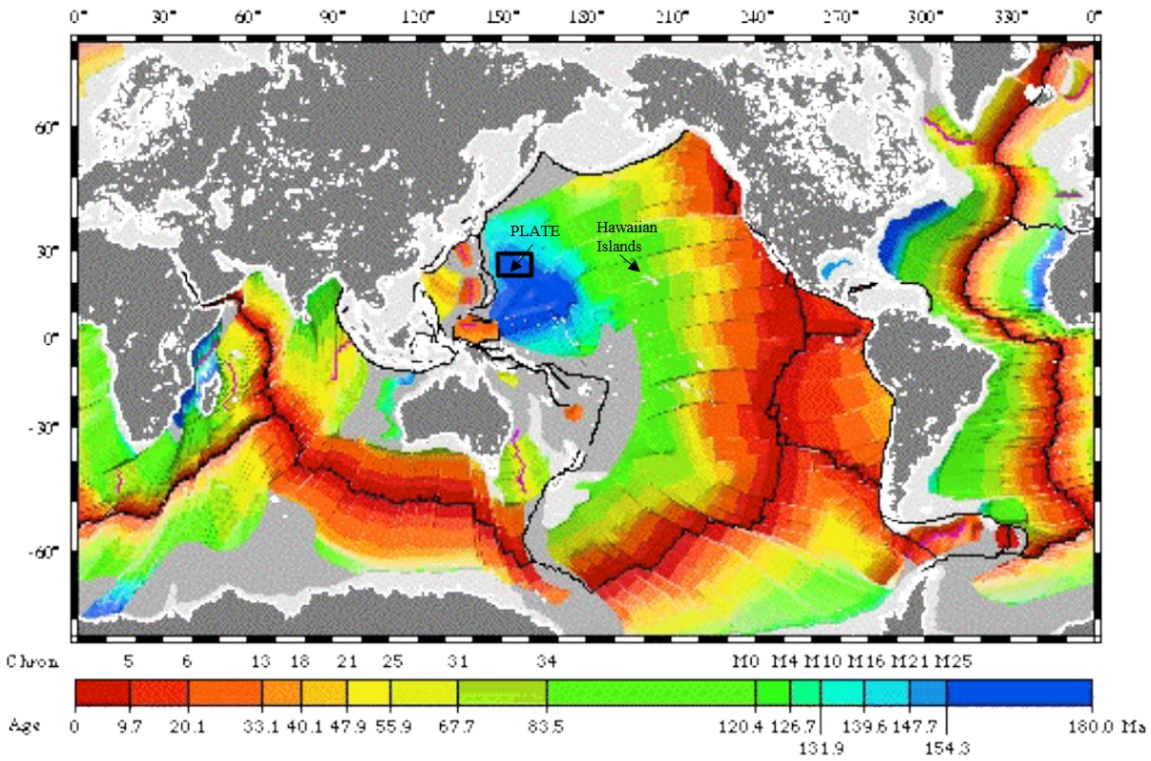

Figure 2. World seafloor age map (Muller et al., 1997). Black rectangle indicates the PLATE project location. Colors indicate the seafloor age as indicated in the legend.

The northwest Pacific was carefully chosen for its uniquely old, 150-160 Ma seafloor (Figure 2) and presence of a magnetic bight, which takes advantage of anisotropic fabric in the lithosphere and asthenosphere to identify the location of the LAB (Sotirov, 2014). Two subarrays were deployed, one along each limb of the magnetic bight, labeled as East and West for simplicity (Figure 3). The magnetic bight near the Shatsky rise contains magnetic isochrons and remnant fabric from an ancient triple junction. The western array records data along the limb where current plate motion and

the ancient westerly spreading direction are near parallel. The eastern array resides on seafloor where ancient spreading direction is approximately perpendicular to current westward Pacific plate motion (absolute plate motion today is 72 °W of North).

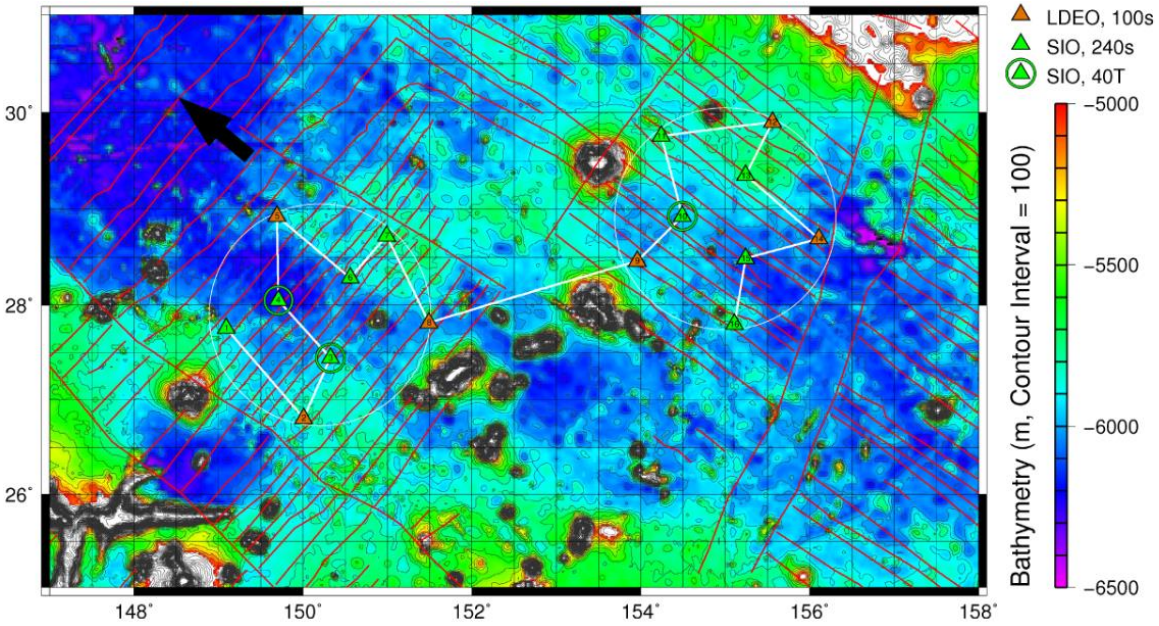

Figure 3. Detailed bathymetry map of the study area. White lines represent the ship track for deployment aboard the R/V Roger Revelle. Numbers in the triangle indicate order of deployment, black arrows represent the general plate movement direction, red lines are magnetic lineations associated with the Japanese and Hawaiian lineation sets. The eastern region is defined by the circle of stations between 153 W and 156 W. The western region is defined by the circle of stations between 149° W an151° W.

1.3 The Conductive Cooling Model in a Semi-Infinite Half Space

New plate material forms at spreading centers where hot molten basalt rises to the surface and solidifies to form oceanic crust. Basalt tends to be hydrated both directly from the melt source and from hydrothermal circulation at the surface. Subsequent spreading pushes older seafloor away as new molten basalt rises at the center. An olivine rich, rigid lithosphere forms beneath the crust and may be dehydrated by the crustal melting process which preferentially partitions water and volatiles quickly to the surface (Karato and Jung 1998). As the plate spreads away from the spreading axis it travels over the asthenosphere getting colder, thicker and denser with time. This process can be modeled by a conductive cooling model of a semi-infinite half space (Parsons and Sclater, 1977). The half-space conductive cooling (HSC) model is parameterized by the selected isotherm which defines the base of the lithosphere. I use the theory (see development in

Appendix E) to predict plate depth, y, as a function of thermal diffusivity (κ) by calculating a range of isotherms as a function of seafloor age (t)

$$\frac{T - T_1}{T_1 - T_0} = erfc\frac{y}{2\sqrt{\kappa t}} \quad . \tag{1}$$

I assume the isotherm of 1350 ° C (Simon et al., 2008) for the temperature defining the base of the lithosphere (T_1) seafloor range of 150-160 Ma, where T_0 is the temperature at the top of the half space, and T is the temperature at the location in question of the half space (Figure 4).

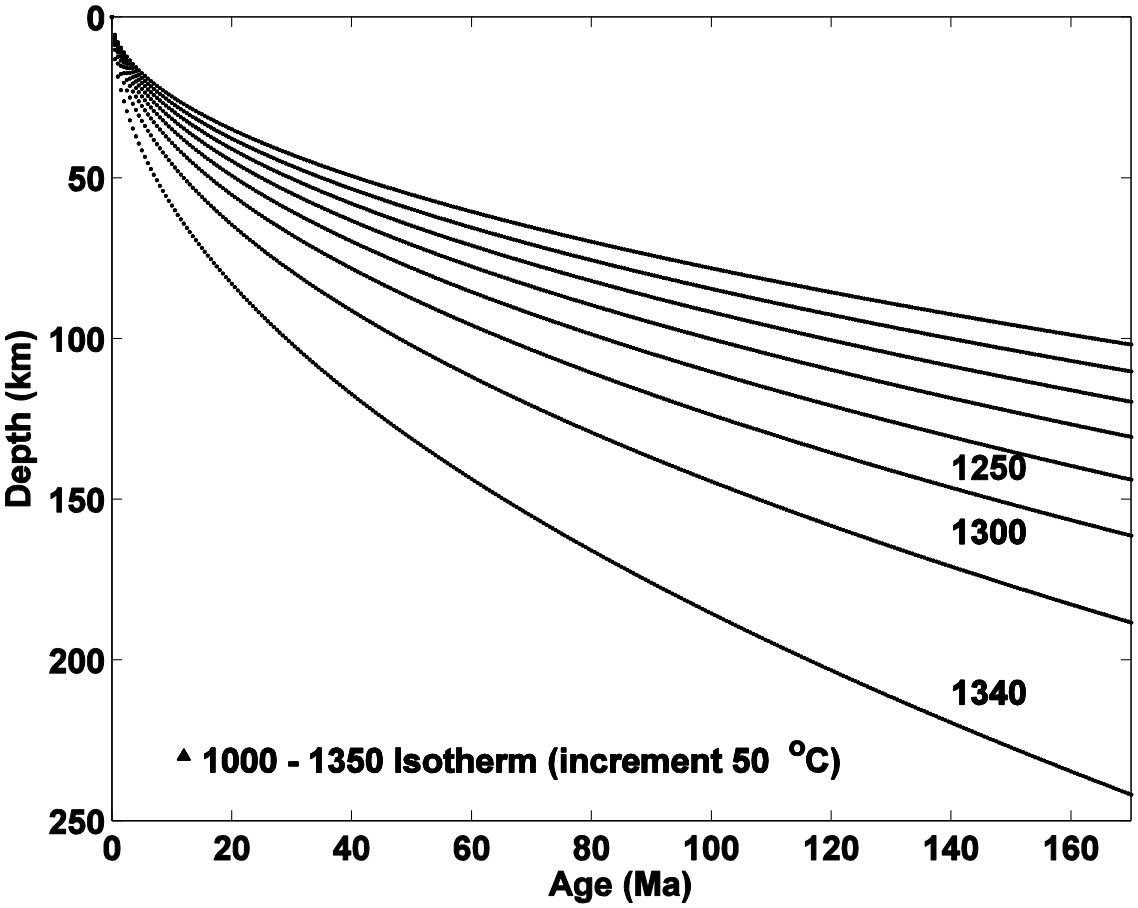

Figure 4. Half space conductive cooling model plotted with isotherms that vary from 1000 °C to 1350 °C, incremented by 50 °C (1340 shown as 1350 is undefined by the denominator).

1.4 Alternate Models

The Plate model (McKenzie, 1967) restricts the depth of the base of the lithosphere by assigning a given value based on external *a priori* information (e.g. 125 km). A model of Global Depth and Heat Flow (GDH1), predicts a hotter lithosphere at depth and a thinner asymptotic limit for the thermal plate signature (Stein and Stein, 1992) than the HSC model. This model can allow for the influence of hotspot swells, hydrothermal circulation, and deeper mantle anomalies.

Small scale convection occurs when local thermal instabilities form across fracture zones where seafloor slabs of differing age may create local instabilities (Richter and Parsons, 1975). The temperature offset between warmer, younger seafloor and older, colder seafloor creates an initial downwelling and a short lived convective cell may develop. The warming of the cold, old lithosphere subsequently thins and raises the base (Huang and Zhong, 2005) where the inclusion of small scale convection and inherent internal heat transfer is less efficient because of lithospheric thickness. Convection either erodes the base of the lithosphere, or heats the lithosphere and increases surface heat flux. Small-scale convection was suggested by numerical modeling which assumes constant heat flow through a natural thermal instability boundary (Doin and Flout, 1996). Small scale convection also does not result in the homogenized mantle temperature predicted by the Plate model, and some studies suggest that internal heating may lead to steeper topography than HSC predicts (Huang and Zhong, 2005). If the conductive cooling model is not sufficient to explain the formation of old lithosphere, then other models and mantle processes may need to be considered.

CHAPTER 2

Marine Seismic Data

2.1 The PLATE project

The seismic data used in the PLATE project were obtained from ocean bottom seismometers deployed in the western Pacific, south east of Japan, southwest of Shatsky rise, and north of Guam (Figure 3). Sixteen seismometers were deployed in two circular arrays, an eastern and western array each ~250 km in diameter. Scripps Institute of Oceanography (SIO) and Lamont Doherty Earth Observatory (LDEO) both contributed instruments (see Sotirov, 2014) as part of OBSIP pool (Ocean Bottom Seismometer Instrument Pool). Instruments were deployed from aboard the R/V Revelle in October 2009, and retrieved on board the R/V Kilo Moana in November 2010. Given the deep ocean depths of the study area, there were a several instrument losses. Four ocean bottom seismometers (OBS) were never recovered (OBS 2, 3, 5, 14) and several others had debilitating technical problems. Several of the recovered instruments timing errors and limited recording lengths. Instruments 6, 9, 10 and 13 only recorded pressure sensor data; OBS's 7, 11, 12 and 15 stopped recording before the year-long deployment ended; OBS 4 had a clock drift, and OBS 8 had a corrupt differential pressure gauge (DPG). The initial data recovery rate was only 43%. Several instrument corrections were applied to the raw data (Sotirov, 2014) to augment data sampling and improve the recovery rate to 55%, and ultimately use data from eleven of the initial sixteen instruments.

The instruments reliably recorded a total of 86 earthquake events at distances ranging from 22° to 90° with a magnitude $\geq$ 6.0 and earthquake depths less than 250 km (Sotirov, 2014). Rays arrive from a broad range of azimuths, though there are fewer arrivals in the northwest back-azimuth (Figure 5).

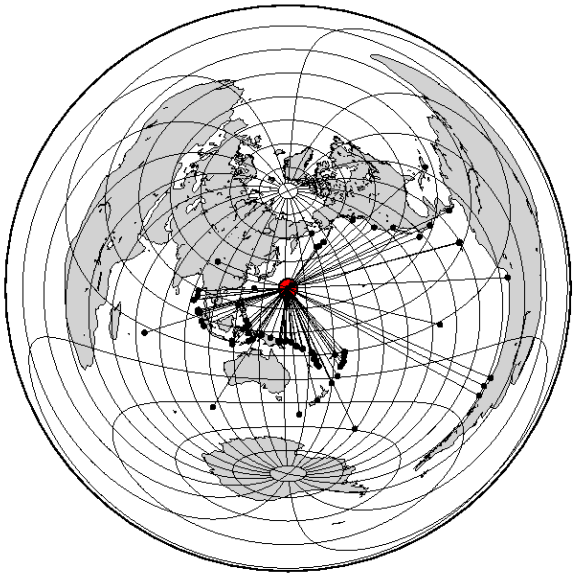

Figure 5. Distribution of 86 events relative to the study area (red square), shown in an equidistant plot. Circles are earthquakes. Lines show the great-circle path between the earthquake event and the experiment location.

2.2 Phase Velocity Data

Standard procedure for OBS data includes an on-board correction of linear clock drift after retrieval of the instruments. Post-processing added necessary non-linear drift correction to LDEO instruments to sync with the SIO instruments. Initial data processing revealed that a few of the OBS's returned pressure data only and no sensor data. Several instrument corrections were performed (Sotirov, 2014) which take into account water reverberations and convert DPG (Differential Pressure Gauge) to vertical data, but this is only valid for periods less than 50 s. Longer period data sense deeper structures. The long period correction was performed to extend the data from 50 s to 143 s to sample deeper depths using the combined components of the DPG data as well as the transverse, radial, and vertical components. We also added a tilt correction and correction for the water

column, yielding 13% more long period data, up to 143 s. Unfortunately, this data is often not within a 95% confidence interval.

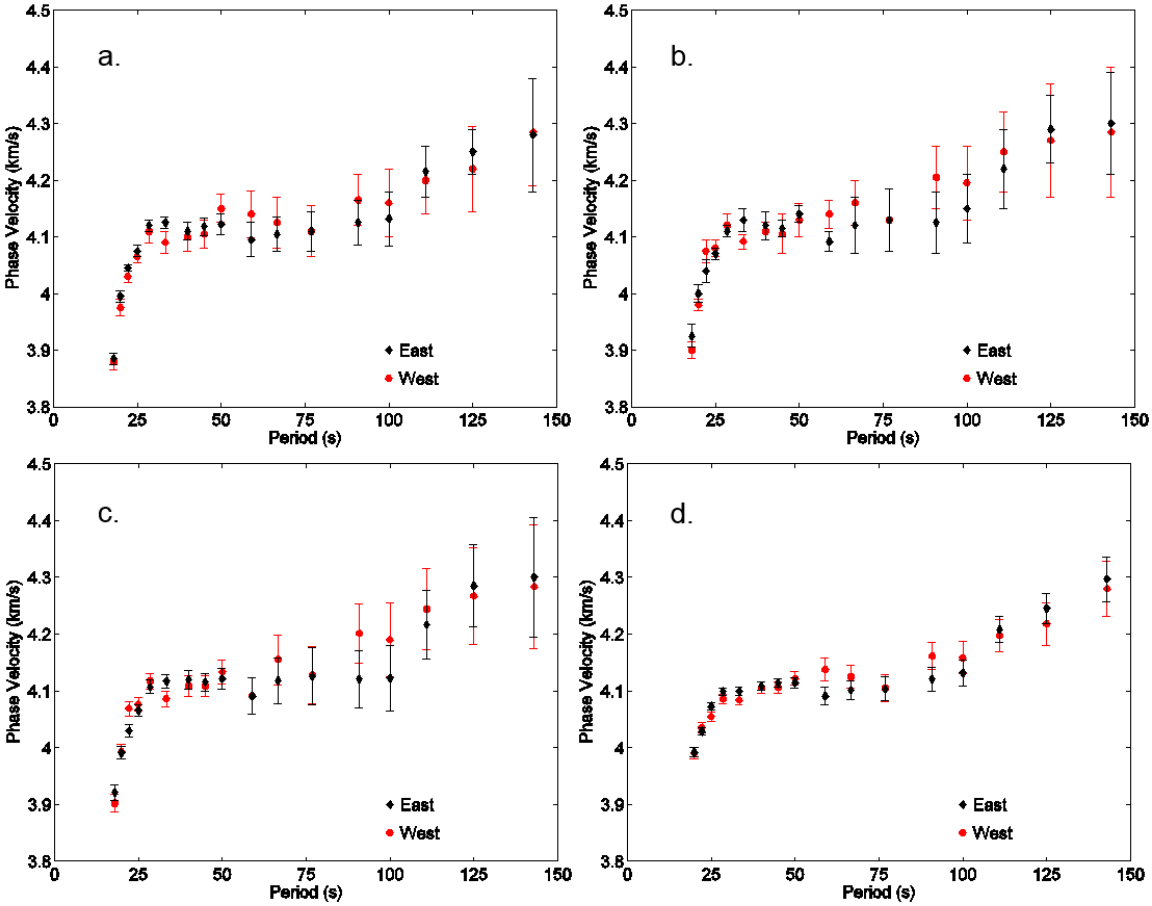

Figure 6. Four different phase velocity data plots, compiled from slightly different Rayleigh wave inversions (Sotirov2014). a) P1 is published in (Sotirov 2014) uses 86 events and the 2 plane wave method, b) P2 is a slightly modified version which uses 86 events in short period (18 s – 50 s) but only 38 events in the longer period. c) P3 is from the original OBS data, limited to 38 events at all period, with two plane wave method, and d) P4 uses the smallest data set with 38 events across 16 periods (20 s – 143). Black diamonds represent the eastern region, red circles the western region, both with 95 % confidence error.

The initial dataset was inverted over the entire study area for each period to produce one dimensional phase velocities (Sotirov, 2014). Since the data control declines in longer periods, two slightly different inversion methods were applied. These velocities were then used as a 1-D *a priori* input to a grid search to estimate separate phase for the two designated study areas of East and West using a grid search. Before inputting phase velocities into the inversion, the raw data were corrected and inverted in previous studies to produce the best resolved phase velocities while minimizing the associated error. Four

slightly different Rayleigh wave inversions were performed to test which combination of corrections yielded the best trade-off between best fit of the data and damping of the resulting phase velocities. Data set P1, as seen in Figure 6.a, utilizes the maximum 86 events recovered from the data at all periods from 18 s – 144 s. The data set P2 in Figure 6.b uses the 86 events only for the short period data from 18 s – 50 s. The long period data utilizes all the corrections but is limited to 38 events. In set P3 (Figure 6.c), periods 18 s – 50 s use the two plane wave approximation. Data set P4 (Figure 6.d) contains the smallest error, but also contains the smallest data set, with only 38 large events across periods 20 s – 143 s. The short period data, up through 50 s, has good back azimuthal distribution and uses the two plane wave method (Forsyth and Li, 2003). The longer period data from 59 s – 143 s uses the single plane wave approximation.

CHAPTER 3

Methods

3.1 Shear Wave Inversion

To estimate the shear velocity structure in the upper mantle of the study area I invert Rayleigh wave phase velocities for shear wave velocities. The inversion is performed around a layered Earth starting model that utilizes *a priori* information from previous studies of old seafloor (e.g. 110+ Ma; Nishimura and Forsyth et. al., 1988, 1989). The inversion uses a forward and inverse problem which iterates the shear velocity structure to produce the best fit between observed $c^{obs}(\omega)$ and predicted $c^{pre}(\omega)$ phase velocities (c) for a range of periods (or frequencies, ω). This approach requires initial estimates of the velocity structure and iteratively refines those estimates to best fit the observed phase velocities. The inversion is 1-D, though I calculate separate models for the two adjacent study areas.

3.2. Starting Models

The inversion revolves around a finite layered Earth model. My starting model is initially based on the IASP95 reference Earth model to create the most general data set. I then modify upper mantle velocities using previous studies for 110 + Ma seafloor (Nishimura and Forsyth, 1989). The shallow crustal structure (Figure 7) in the upper 11 km is comprised of the water column and upper and lower crust using velocities obtained from ambient noise correlation studies (Takeo et al., 2014).

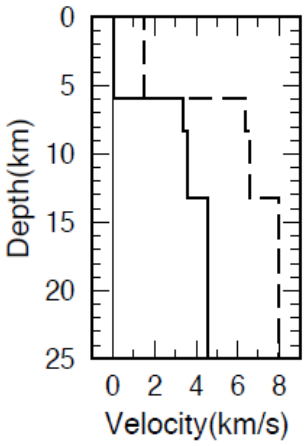

Figure 7. Shallow crustal structure in the upper 5 km from ambient noise correlations (Takeo et al., 2014). The solid line is shear wave velocities, dashed line represents P wave velocities.

In the inversion I assume the lithospheric material is a Poisson solid, and so fix the Vp/Vs ratio to $\sqrt{3}$. Rayleigh waves consist of the combination of P and vertical S energy. Thus I allow both Vp and Vs wave velocities to vary between iterations from the original starting model.

3.3 The Forward Problem

In the forward model, the program reads in the layered Earth starting model of P and S wave velocities and material density. The first step of the program (Saito, 1988)

produces phase velocities for this starting model and solves for partial derivatives between Vs and

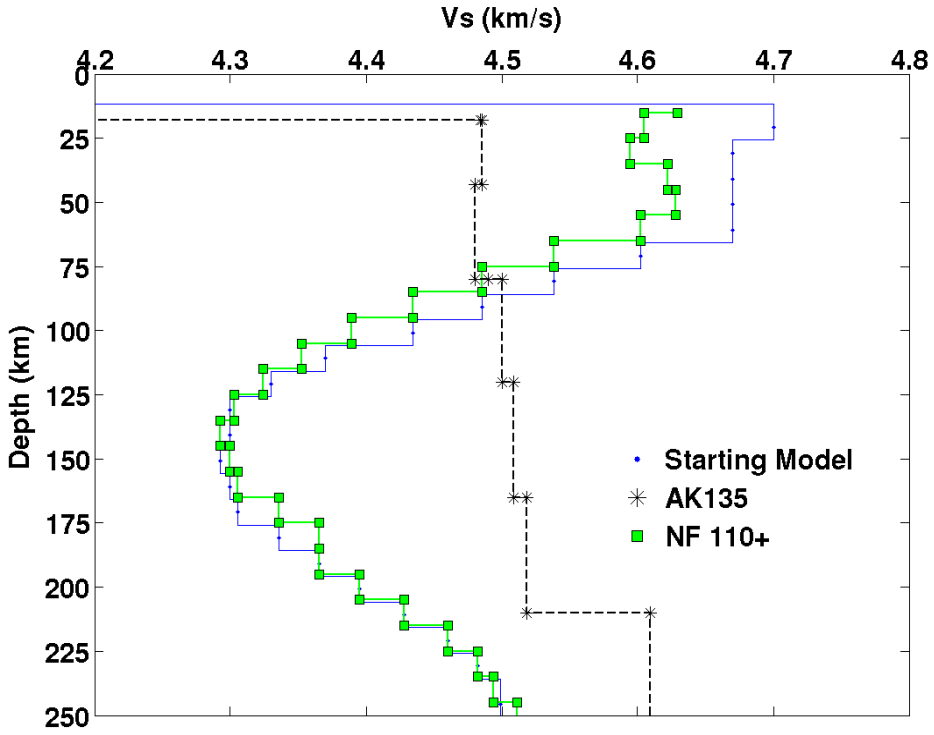

Figure 8. Input Vs Starting model. The dashed gray line with stars is the global reference model AK135. The solid green line with squares represents land station receiver function data on 110 +Ma seafloor (Nishimura and Forsyth, 1989). The solid blue line with dots is the composite input Vs starting model applied to my inversions.

C(ω) for Rayleigh waves traveling over a curved Earth surface. The partial derivatives are compiled from the energy integral

$$w^2 I_1 = I_2 \quad . \qquad (2)$$

Given by the eigenfrequencies, w(k), and the eigenfunctions, for a given k and Earth model, I1 and I2:

$$I_1 = \int_{-\infty}^{H} \rho y_1^2 dz \tag{3}$$

$$I_2 = \int_{-\infty}^{H} (\frac{1}{L} y_2^2 + k^2 N y_1^2) dz \quad . \tag{4}$$

Equations (3) and (4) produce the partial derivatives using the eigen frequencies by a ratio of phase velocity to group velocity.

The forward problem yields the predicted phase velocities and subsequent partial derivatives for each layer (z) in the model

$$(\frac{\delta c(z)}{\delta \beta})_R = (\frac{\delta c(z)}{\delta \beta} + \sqrt{3}\frac{\delta c(z)}{\delta \alpha}) h(z) \quad . \tag{5}$$

3.4 The Inverse Problem

The inverse method works to close the inversion loop. The program reads in the predicted phase velocity data obtained from the forward model as input and solves for shear wave velocities. To resolve the most accurate model, the inversion evaluates the difference between the observed phase velocity data (C^{obs}) and the predicted velocities (C^{pre}) in a least squares sense for a given Vs starting model

$$\sqrt{(c^{obs} - c^{pre})^2} \quad . \tag{6}$$

Successive iterations adjust the starting Vs model and re-evaluate the fit between phase velocities. My inversion performs three iterations which produce a best-fitting shear velocity model. The fit of the inversion is shown by the final residuals. The model parameters are shear wave velocity, β(z), for 43 layers which vary thickness from 2 km at the top and 50 km at the bottom. $\frac{\delta c}{\delta \beta}$ relates the data, the observed phase velocities, to the model parameters over 17 periods from 18 s to 143 s.

$$\begin{bmatrix} c_1(w) \\ c_2(w) \\ . \\ . \\ c_{17}(w) \end{bmatrix} = \begin{bmatrix} \frac{\delta c_1}{\delta \beta_1} & \frac{\delta c_1}{\delta \beta_2} & \cdots & \frac{\delta c_1}{\delta \beta_{43}} \\ \frac{\delta c_2}{\delta \beta_1} & \frac{\delta c_2}{\delta \beta_2} & \cdots & \frac{\delta c_2}{\delta \beta_{43}} \\ \cdots & \cdots & \cdots & \cdots \\ \cdots & \cdots & \cdots & \cdots \\ \frac{\delta c_{17}}{\delta \beta_1} & \frac{\delta c_{17}}{\delta \beta_2} & \cdots & \frac{\delta c_{17}}{\delta \beta_{43}} \end{bmatrix} \begin{bmatrix} \beta_1(z) \\ \beta_2(z) \\ . \\ . \\ \beta_{43}(z) \end{bmatrix} \quad . \qquad (7)$$

The peak depth of sensitivity for Rayleigh waves is approximately 4/3 period, as shown in Figure 22 which demonstrates overlap in sensitivity between periods. This effect is stronger at deeper depths and long periods where Rayleigh wavelengths are longer.

A priori model parameters in the form of damping minimize the difficulty in finding the solution to an underdetermined problem. I test a variety of damping parameters which consider the diagonals (minimum length) and off diagonals (curvature) of the covariance matrix (Equation 6) and compare the results below. The model covariance matrix, C_{mm}, is represented as

$$C_{mm} = \sigma_m^2 I \qquad (8)$$

where the data covariance matrix, Cnn, has diagonal elements corresponding to each data value of phase velocity and sigma n. The full damped least squares inversion is given by

$$\Delta m = (G^T C_{nn} G + C_{mm}^{-1})^{-1} (G^T C_{nn}^{-1} \Delta d - C_{mm}^{-1}(m - m_0)) \qquad (9)$$

Where Δm is the change to the model, Δd is the difference between predicted and observed phase velocity data, and the G matrix is comprised of partial derivatives, m is the current model, and m_o is the original model, which is then iterated. The terms in the farthest left parentheses are inverted using inversion routines from Numerical Recipes (Press et al., 1986). The final Δm is compared to the original starting model to resolve the shear wave velocity model with the best fit to the data in a least squares sense.

3.5 Error Analysis

Errors are computed for vertical depth and horizontal velocities, but the errors are highly correlated with one another. Errors in depth are obtained from analyzing the rank of individual layers of the resolution matrix. Rank is a measure of the number of independent pieces of information obtained by the inversion. Each rank of the layers is summed until rank equals one, and indicates how many layers are required to produce one independent piece of information, providing an estimate of error in depth. This determines the vertical thickness of the error boxes of the shear wave velocity curves shown in Figure 20 and Figure 21. Velocity errors are compiled for each group of layers with rank equal to one. The off diagonals of the covariance matrices are summed and averaged over the number of layers in each box group to resolve the average error in velocity over that depth range. The standard deviation of the average velocity is the product of twice the square root of the variance of the average velocity to resolve 95% confidence.

Phase velocities input into the inversion of this study are not raw data; the raw data were corrected and inverted in previous studies to produce our input phase velocities (Sotirov, 2014). Errors in the input data are not formally propagated through the inversion. Instead, the various phase velocity dat sets in Figure 6 use different number of events and use either single or two plane wave methods in the short and long period data

3.6 Computational Inversions

To explore the effects of the specific inversion technique on the final shear wave velocity estimates, I run three slightly different inversion programs while varying relevant parameters. These parameters include data damping, model damping (c_{mm}), minimum curvature, minimum length, as well as the starting Vs model and input phase velocity data. I set all parameters constant and vary one parameter at a time in each set of inversions (for full details see Appendix C). The Saito (1988) inversion is advantageous because it accounts for the curvature of the Earth, which can be an important factor for long Rayleigh wave travel distances. Inversion 1 runs through three iterations, assuming that the data samples a Poisson solid with minimal density variation and constant water column and crustal thickness, and maintains a P to S wave ratio of $\sqrt{3}$, but does not

include a parameter for curvature smoothing of the off diagonals (curvature parameters). Inversion 2 allows for curvature, and only runs through 2 iterations. The second inversion is a desirable update to the first because of its ability to turn smoothing on and off, vary data damping parameters, model damping parameters, and manipulate the ratio of P to S wave as well as density to S wave velocity. Additionally, inversion 2 seeks to further constrain the data by adding an additional correctional term which is dependent on the resolution matrix and the amount of change applied between inversions.

Inversion 3 is the ultimate attempt at producing optimized data. This inversion decidedly works best for the PLATE data set when I make P wave, S wave, and density values independent from each other; furthermore, this inversion is performed with 10 iterations. Inversions 2 and 3 allowed the shallow structure water column and crust to vary as per the inversion requirements, but with different input values as compared to Inversion 1 and as shown in Figure 7. The starting model from inversion 1 keeps densities in the water column and crust fixed, along with P wave velocities from 1.5 km/s to 6.9 km/s, and S wave velocities in the crust from 2.0 km/s to 3.7 km/s. The second inversion uses these same values, but is allowed to vary as per the inversion requirements. The third inversion includes starting model P wave crustal velocities from 4.3 to 6.9, and S wave velocities from 2.0 km/s to 3.8 km/s; these are markedly higher than the structure in figure-crust-input-a but are then allowed to vary.

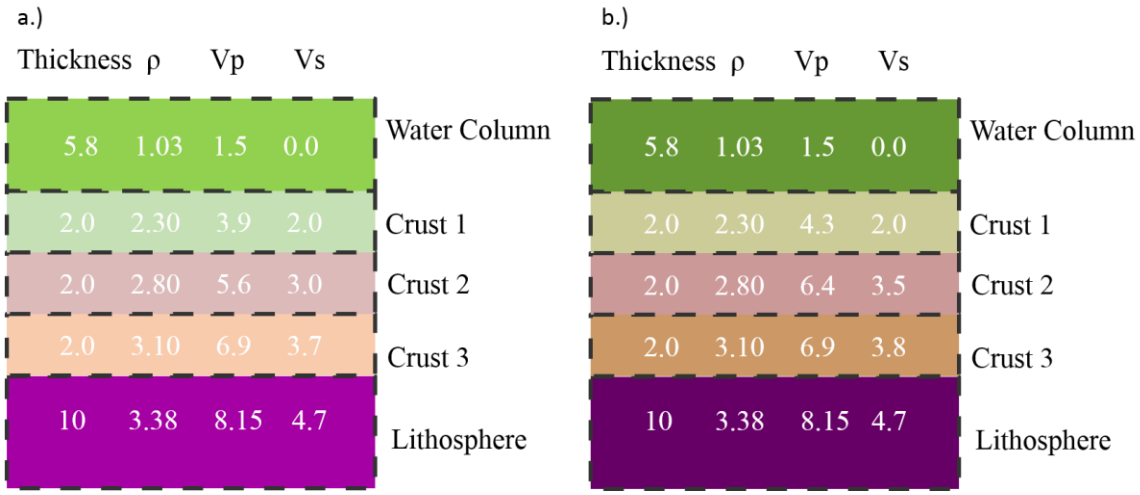

Figure 9. Shallow structure starting model for a) inversion 1 and 2, and b) for inversion 3.

All the models optimize the Root Mean Square (RMS) fit to the observed phase velocities. RMS is calculated as the sum of the residuals, normalized by standard deviation, squared, and then divided by the number of periods, all of which are squared again

$$\mathrm{RMS} = \sqrt{\frac{\sum \left(\frac{\text{obs-pred}}{\sigma}\right)^2}{\mathrm{nobs}}} \quad . \qquad (10)$$

The misfit of the data is, in part, a function of the damping parameters used. After running the model with a range of damping parameters, Iselect the damping parameter that minimizes misfit.

Chapter 4

Shear Wave Velocity Results

Shear wave velocity results are dependent upon starting models and damping parameters used in the inversion, as well as the input parameters of model damping, data damping, minimum length, curvature, and phase velocities. To determine the best resolved velocity structure of my study area, I test a variety of starting shear velocity models, phase velocity inputs, modeling damping and data damping parameters.

I found that 4.7 km/s has the best fit with the data and decided to use this velocity at lithospheric depths from 12 km to 65 km for subsequent tests.

While holding the starting model fixed, I also vary the input phase velocities (Figure 6) as part of the inverse problem. In the first case, with Inversion 1 and phase velocity P1, I use a constant starting model, with curvature, smoothing, and data damping turned off. I find that, when systematically increasing model damping, the trade-off curve (Figure 10.f) indicates that the optimal damping parameter occurs at 0.1 km/s as shown in Figure 10.d which reduces the misfit in the east and west regions. The eastern region displays a shear wave velocity high of 4.76 km/s from 20 km to 60 km. A negative velocity gradient is observed from 65 km to 140 km depth reaching a minimum of 4.28 km/s. The western region extends to a maximum of 4.80 km/s at 30 km, followed by a negative velocity gradient from depths of 75 km to 140 km and higher minimum of 4.40 km/s as compared to the eastern region.

		East					West				
		Vs Max		Negative Gradient of Vs			Vs Max		Negative Gradient of Vs		
Inv	Phase Vel.	Vs Max (km/s)	Depth (km)	Vs Min (km/s)	Start Depth (km)	LAB (km)	Vs Max (km/s)	Depth (km)	Vs Min (k/s)	Start Depth (km)	LAB (km)
1	P1	4.76	20-60	4.28	65	140	4.8	30	4.4	75	140
1	P2,P3	4.72	30-75	4.3	75	150	4.72	30	4.3	75	150
1	P4	4.70	50	4.3	50	150	4.70	50	4.3	50	150
2	P1	4.7	75	4.3	75	150	4.8	65	4.35	65	150
2	P2,P3	4.7	65	4.25	65	125	4.7	65	4.25	65	125
2	P4	4.71	30	4.25	30	125	4.75	60	4.35	65	150
3	P4	4.7	30	4.3	65	140	4.8	35	4.33	35	205

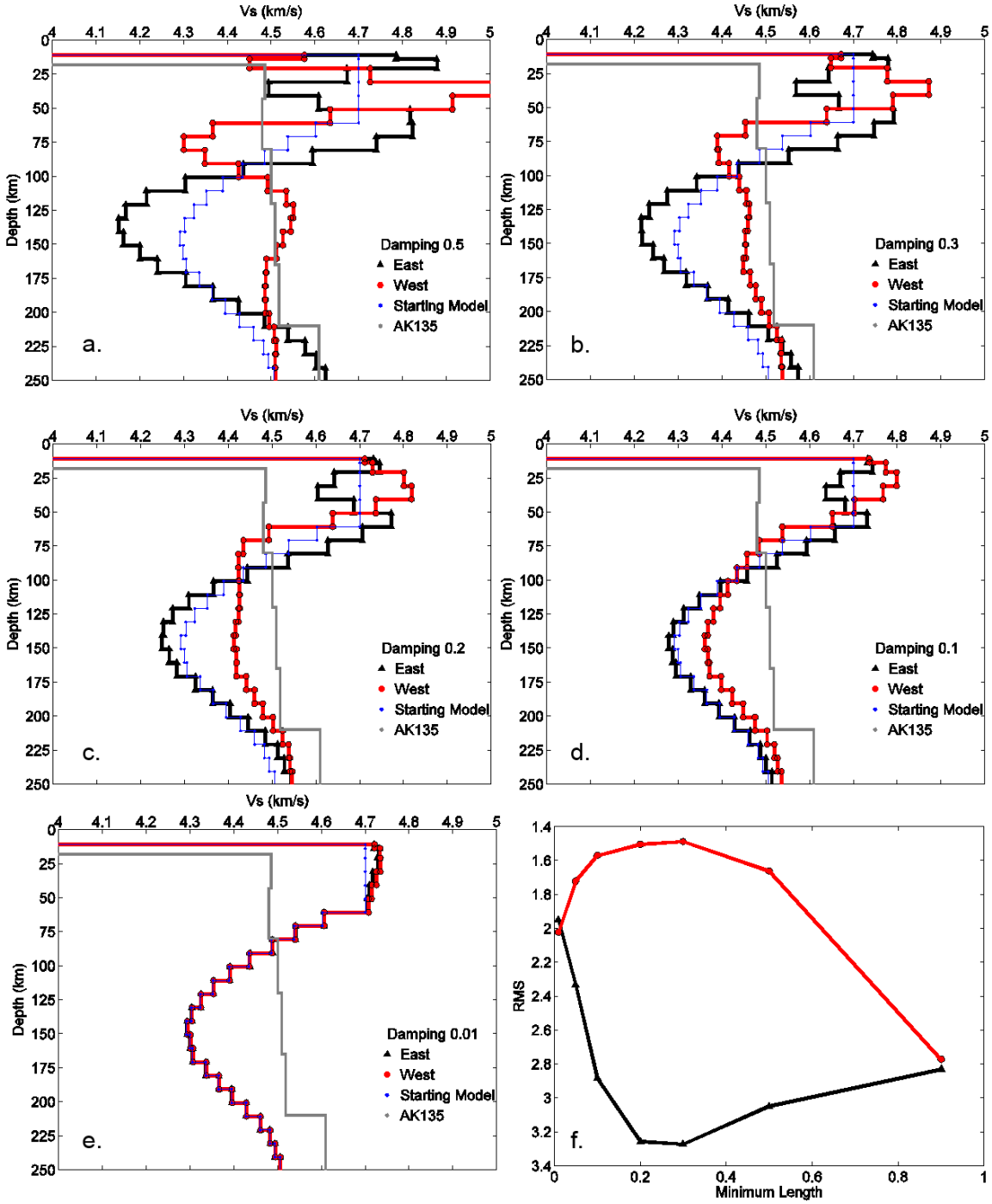

Figure 10. a-e) Results from tests run with inversion 1 and phase velocity data set P1. Red circles indicate the western region, black triangles the eastern region, blue dots the input Vs starting model, and the gray line the global Earth reference model AK135. Each window displays increased damping from 0.5(a), 0.3(b), 0.2 (c), 0.1(d) to 0.01 (e). f) the trade-off curve between minimum length (model damping) and misfit calculated by equation (10).

Next, I apply the same starting model as in the first test, as well as the same range of model damping parameters, curvature, smoothing, and no data damping with Inversion 1 but test phase velocities P2 and P3 (Figure 6.b,c), respectively as shown below in Figure 11 and Figure 12. Results in Figure 11 and Figure 12 yield similar results, both in their velocity structure and misfit. The regions are nearly identical within error when the optimal damping parameter of 0.1 km/s is considered. The upper structure appears pinned to the staring model with a maximum of 4.72 km/s at 30 km depth. A negative velocity zone extends from 75 km to a minimum at 150 km at 4.3 km/s. While the two regions seem slightly different, they are not resolvable differently within error.

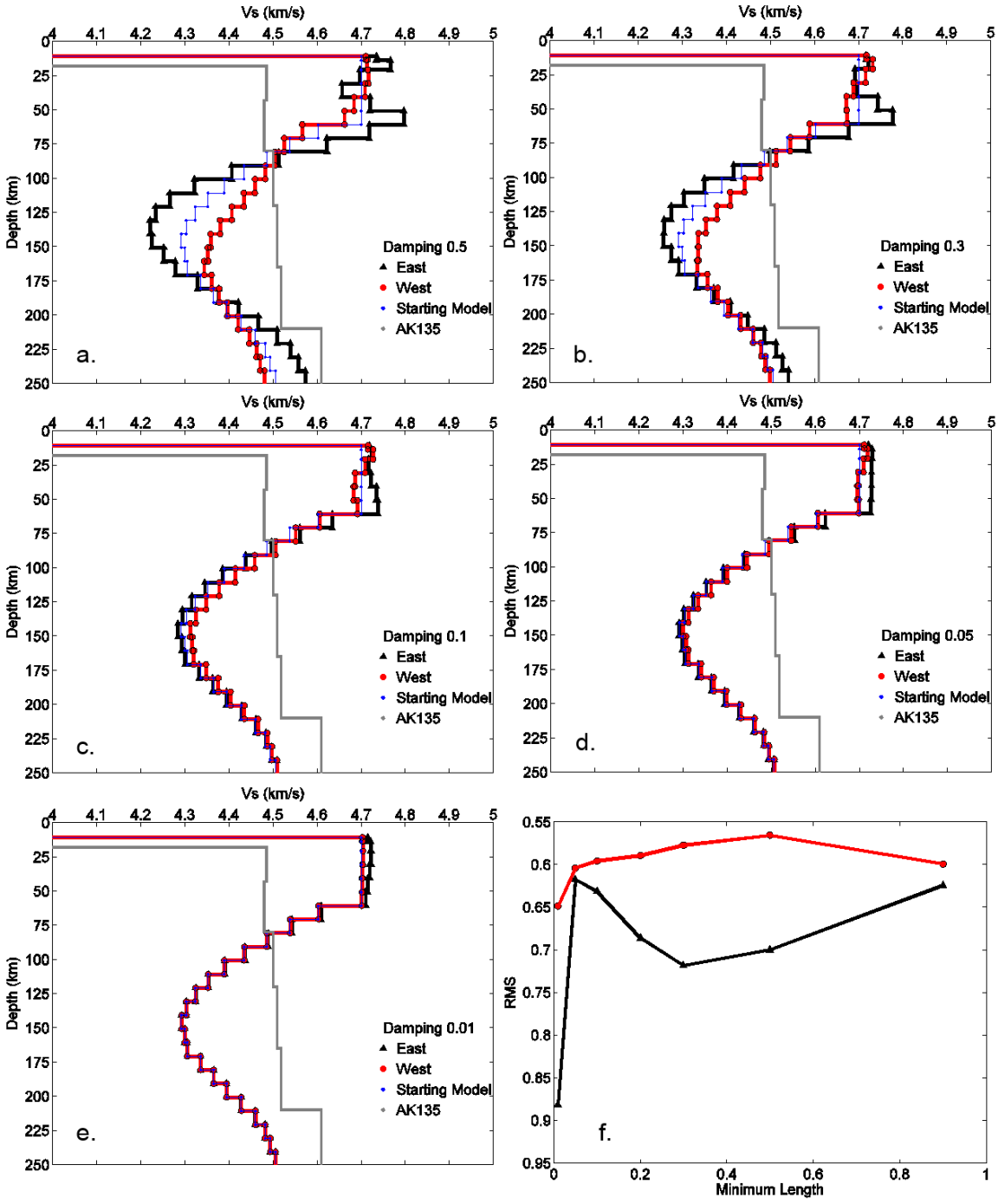

Figure 11. a-e) Results from tests run with inversion 1 and phase velocity data set P2. Red circles indicate the western region, black triangles the eastern region, blue dots the input Vs starting model, and the gray line the global Earth reference model AK135. Each window displays increased damping from 0.5 (a), 0.3 (b), 0.1 (c), 0.05 (d), to 0.01. (e) f) the trade-off curve between minimum length (model damping) and misfit calculated by equation (10).

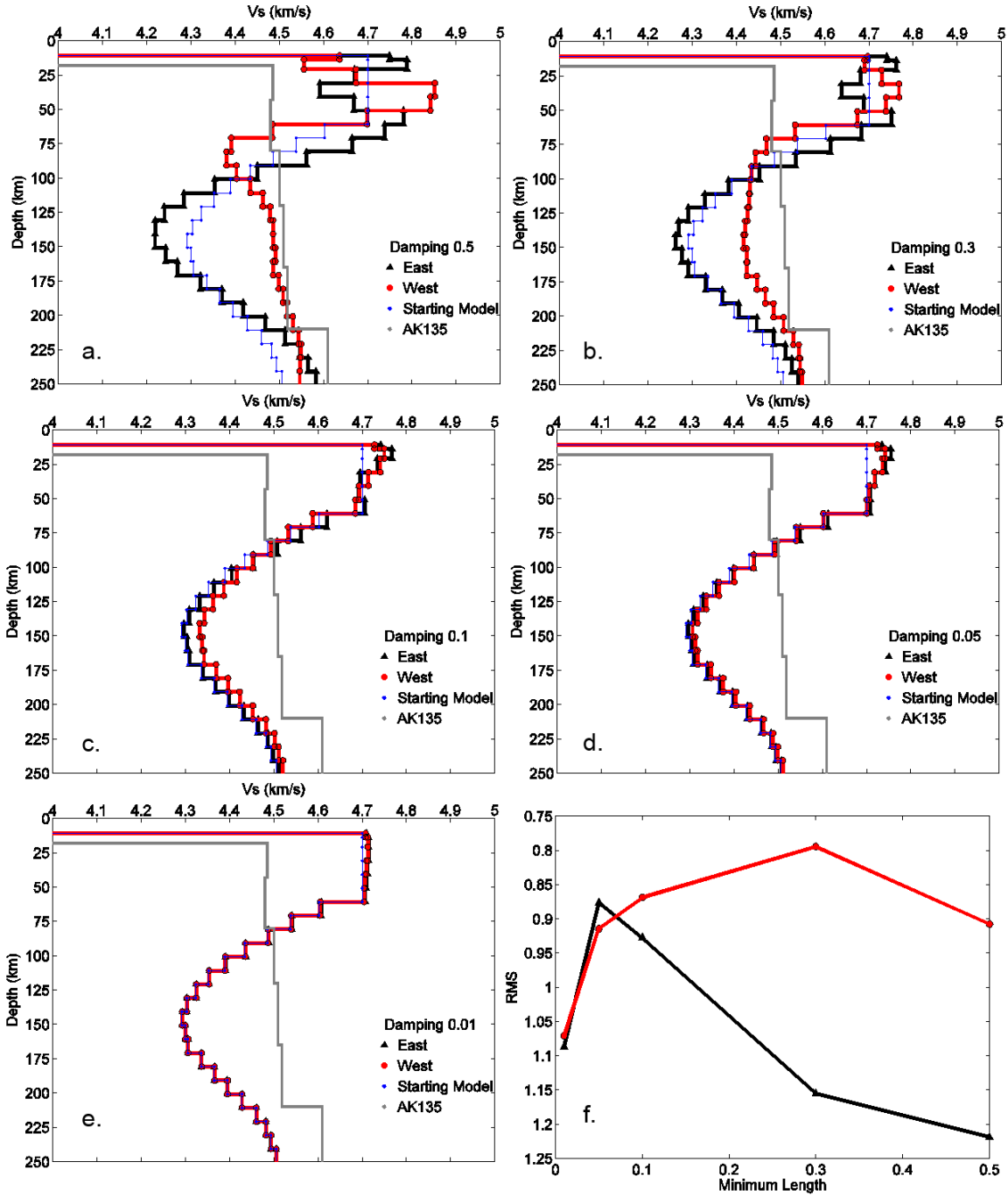

Figure 12. a-e) Results from tests run with inversion 1 and phase velocity data set P3. Red circles indicate the western region, black triangles the eastern region, blue dots the input Vs starting model, and the gray line the global Earth reference model AK135. Each window displays increased damping from 0.5 (a), 0.3 (b), 0.1 (c), 0.05 (d), to 0.01.(e). f) the trade-off curve between minimum length (model damping) and misfit calculated by equation (10).

Inversion 1 with data set P4 (Figure 13) has the same starting model, varied model damping, lack of data damping and smoothing. It results in a similar velocity

structure as in Figure 12, but with steeper velocity gradients. The best fit model requires damping of 0.1 km/s (Figure 13.f), which reaches a maximum velocity of 4.70 km/s at 50 km, and a minimum at 4.30 km/s at 150 km in both regions.

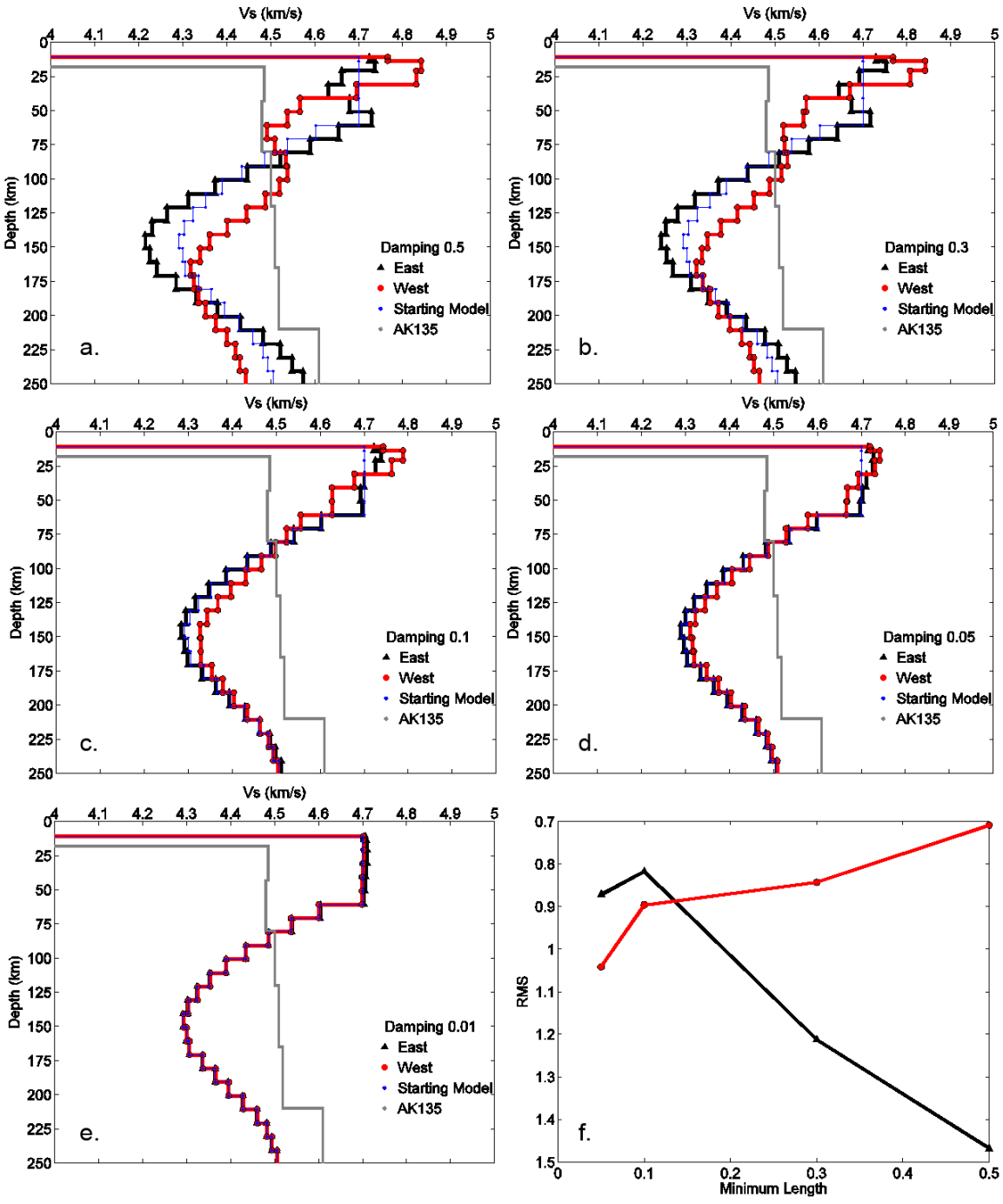

Figure 13. a-e) Results from tests run with inversion 1 and phase velocity data set P4. Red circles indicate the western region, black triangles the eastern region, blue dots the input Vs starting model, and the gray

line the global Earth reference model AK135. Each window displays increased damping from 0.5 (a), 0.3 (b), 0.1 (c), 0.05 (d), to 0.01 (e). f) the trade-off curve between minimum length (model damping) and misfit calculated by equation (10).

Results from Inversion 1 help to constrain the starting model and predict a basic result which is subsequently modified for a better fit in Inversion 2. The next set of inversions use Inversion 2 and use the same starting model as in Inversion 1. I again test all four phase velocity data sets (Figure 6) independently, while systematically varying model damping parameters. The tests include no data damping, continue to assume the structure is a Poisson solid, and have maximum smoothing and curvature. The first subset of tests from this inversion looks at results when phase velocity set P1 (Figure 6.a) is applied, and manages to find solutions between the eastern and western regions when they converge with a damping parameter of 0.1 km/s based on analysis of the misfit of the test in (Figure 14.f). Figure 14.c shows the shallow structure of the eastern region closely follows the starting modeling at 4.7 km/s. A negative velocity gradient extends from 75 km to a minimum velocity of 4.3 km/s at 150 km. The western region indicates a distinct need for higher velocities in the upper structure which stretch to 4.8 km/s at 65 km. The low velocity zone occurs at 100 km and a faster velocity of 4.35 km/s as compared to the east. Progressively less dampened models display marked instability (Figure 14.a,b), with minimum and maximum velocities well outside realistic bounds, and indicate that the solution has not yet converged. Any additional damping stifles the data set and mirrors the starting model (Figure 14.d), and is not informative based on the unbalanced minimum on the trade-off curve.

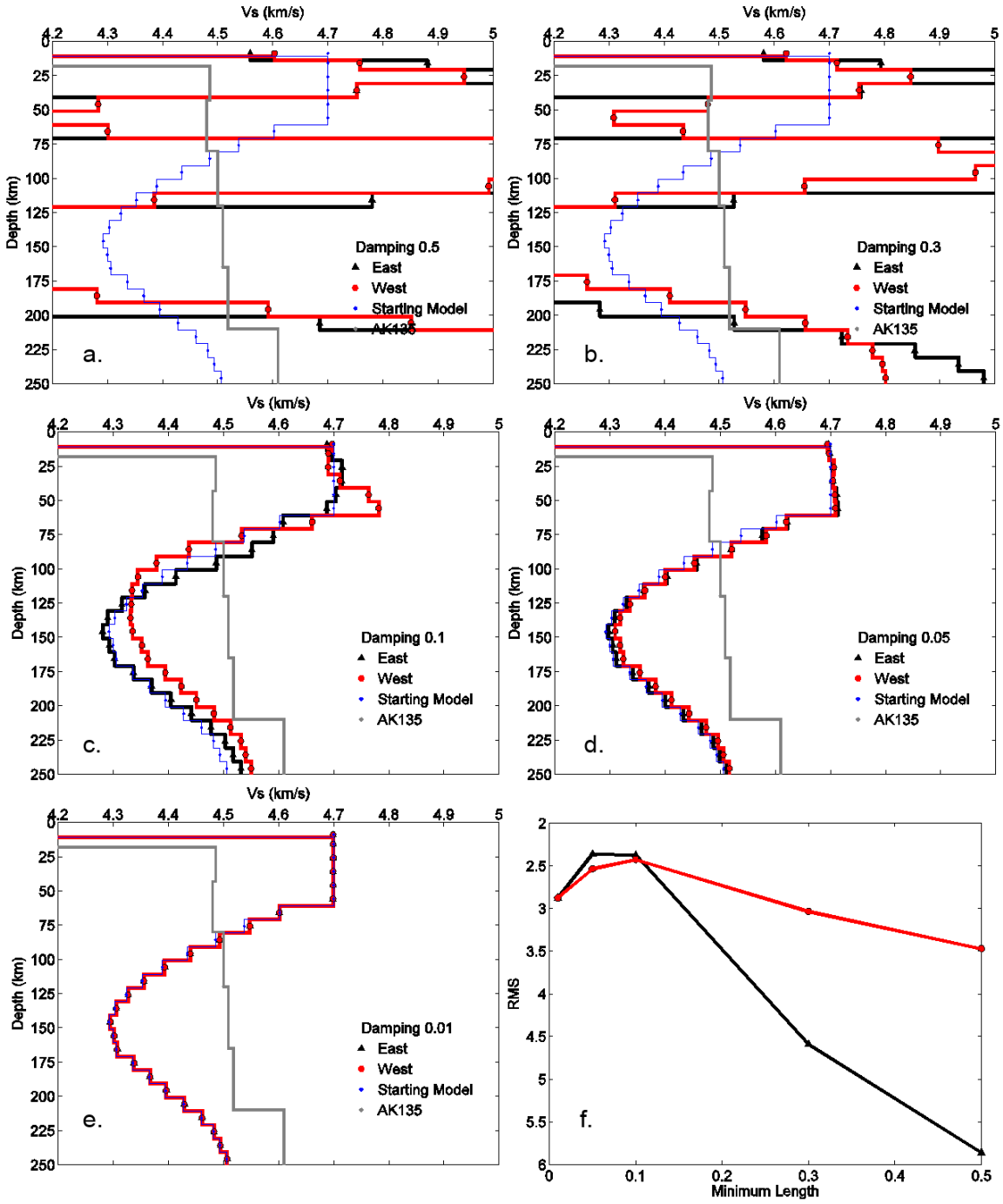

Figure 14. a-e) Results from tests run with inversion 2 and phase velocity data set P1. Red circles indicate the western region, black triangles the eastern region, blue dots the input Vs starting model, and the gray line the global Earth reference model AK135. Each window displays increased damping from 0.5 (a), 0.3 (b), 0.1 (c), 0.05 (d), to 0.01 (e). f) the trade-off curve between minimum length (model damping) and misfit calculated by equation (10).

The second and third subset of tests run with Inversion 2 look at the results when phase velocity sets P2 and P3 are independently applied (Figure 15, 16). Examination of both of these test subsets yield similar results to when they were performed with inversion 1 (Figure 11, Figure 12) and have not yet converged. In Figure 15.f, the uniform misfit for both regions further supports this theory, although the higher RMS in the eastern region is resultant from the better data coverage and return in this region of the array. A reasonable damping of 0.1 km/s, figure 15.c, shows a maximum shear wave velocity of 4.7 km/s at 65 km depth and extends to a minimum of 4.25 km/s at 125 km depth in a negative velocity gradient.

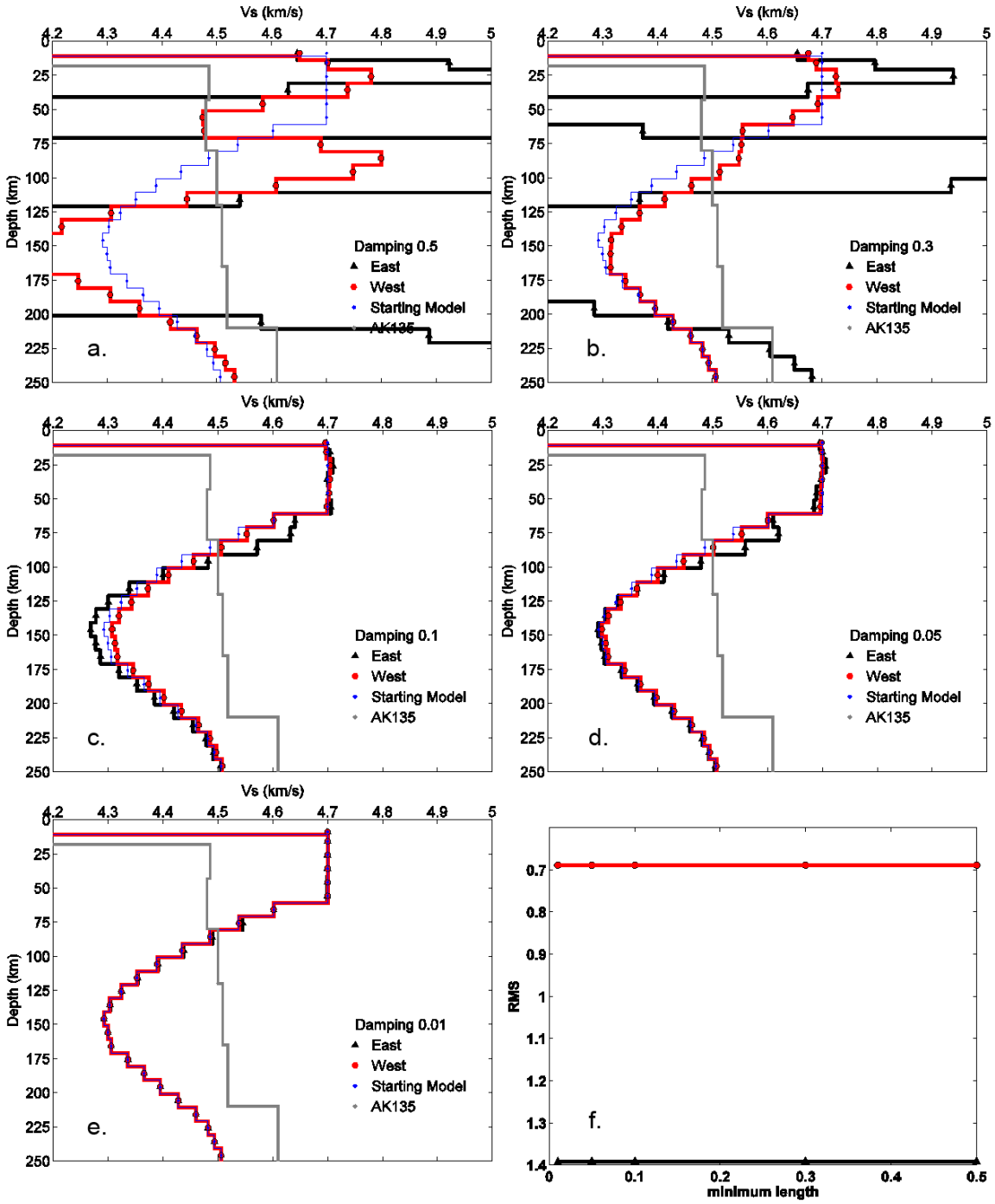

Figure 15. a-e) Results from tests run with inversion 2 and phase velocity data set P2. Red circles indicate the western region, black triangles the eastern region, blue dots the input Vs starting model, and the gray line the global Earth reference model AK135. Each window displays increased damping from 0.5 (a), 0.3 (b), 0.1 (c), 0.05 (d), to 0.01 (e). f) the trade-off curve between minimum length (model damping) and misfit calculated by equation (10).

Comparatively, phase velocities from Figure 16.d show a more resolved trade-off curve. The sharp change in gradient is most likely fixed by adding additional damping parameter tests into the negative and positive gradients in both regions. While the trade-off curves between the two regions are proportional to each other, the western region has a broader range and uniformly smaller RMS, which I expect based on the data coverage rate of the area. Regardless, the optimal damping parameter for both regions is 0.1 km/s (Figure 16.c), as has been true with most tests. Results are similar to those found in Figure 15, with slightly higher minimum velocities of 4.3 km/s and lower maximums of 4.7 km/s. Both regions closely follow the starting model and cannot be well-resolved within error.

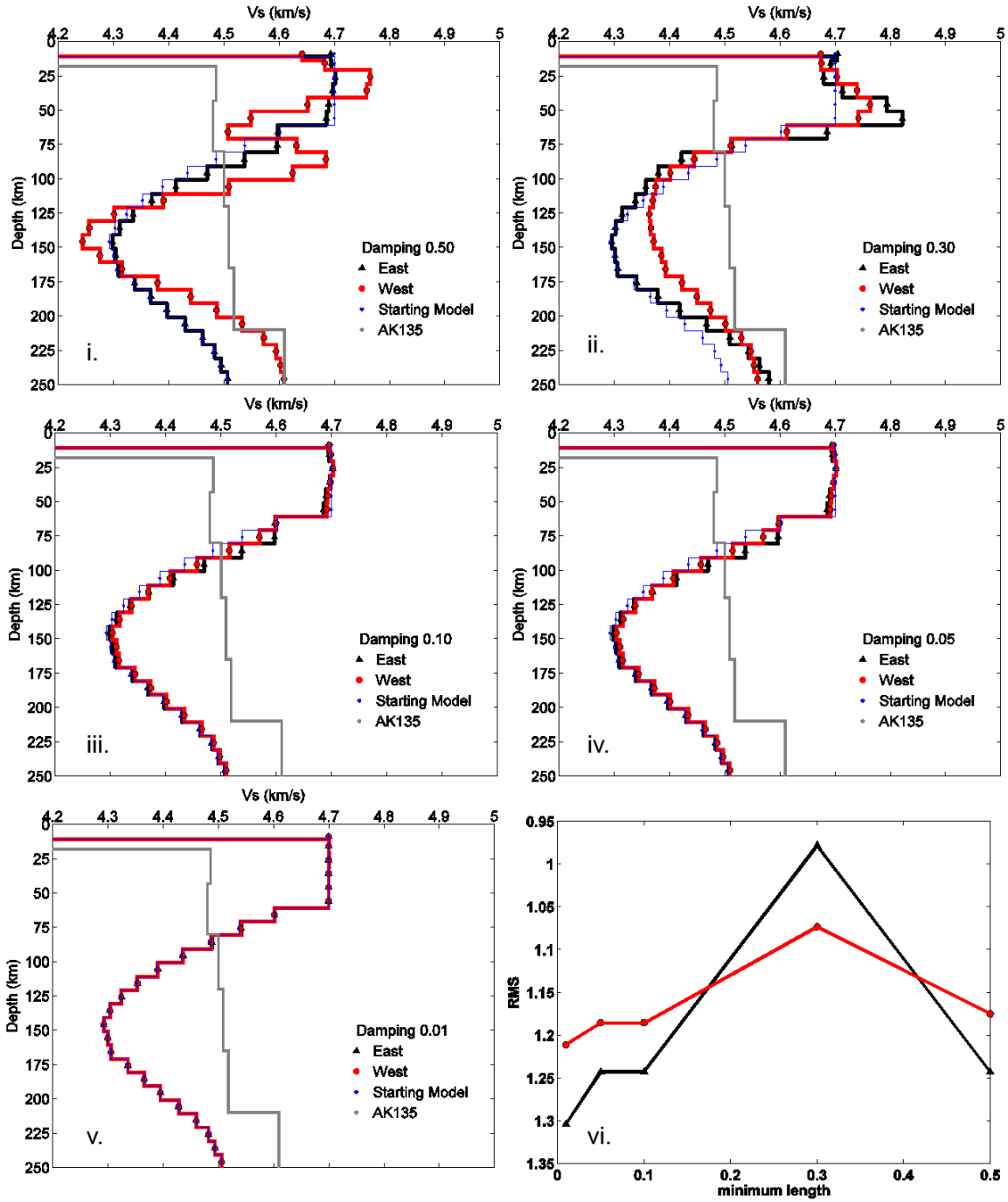

Figure 16. a-e) Results from tests run with inversion 2 and phase velocity data set P3. Red circles indicate the western region, black triangles the eastern region, blue dots the input Vs starting model, and the gray line the global Earth reference model AK135. Each window displays increased damping from 0.5 (a), 0.3 (b), 0.1 (c), 0.05 (d), to 0.01 (e). f) the trade-off curve between minimum length (model damping) and misfit calculated by equation (10).

Finally, I apply phase velocity set P4 (Figure 6.d) to Inversion 2 in Figure 17, where I expect and see the best results between the first two inversions across all 4 phase velocity sets because this dispersion curve shows the smoothest changes in phase velocity between period. The trade-off curve displays a concave up curve. I select the optimal damping parameter of 0.1 km/s, as seen in Figure 17.f. The eastern region has an increasingly large RMS with additional damping, since the data is already well constrained for the area. The region, as shown in Figure 17.c reaches a maximum of 4.71 km/s at 30 km. A negative velocity gradient extends to 125 km depth at 4.25 km/s. The western region shows a marked shift towards higher velocities, with a maximum up to 4.75 km/s at 60 km, and a negative velocity gradient from 65 km to 150 km with a minimum of 4.35 km/s. However, while the velocity change difference is smaller in the west as compared to the east, the velocity change occurs over a much shorter depth interval and with steeper gradients.

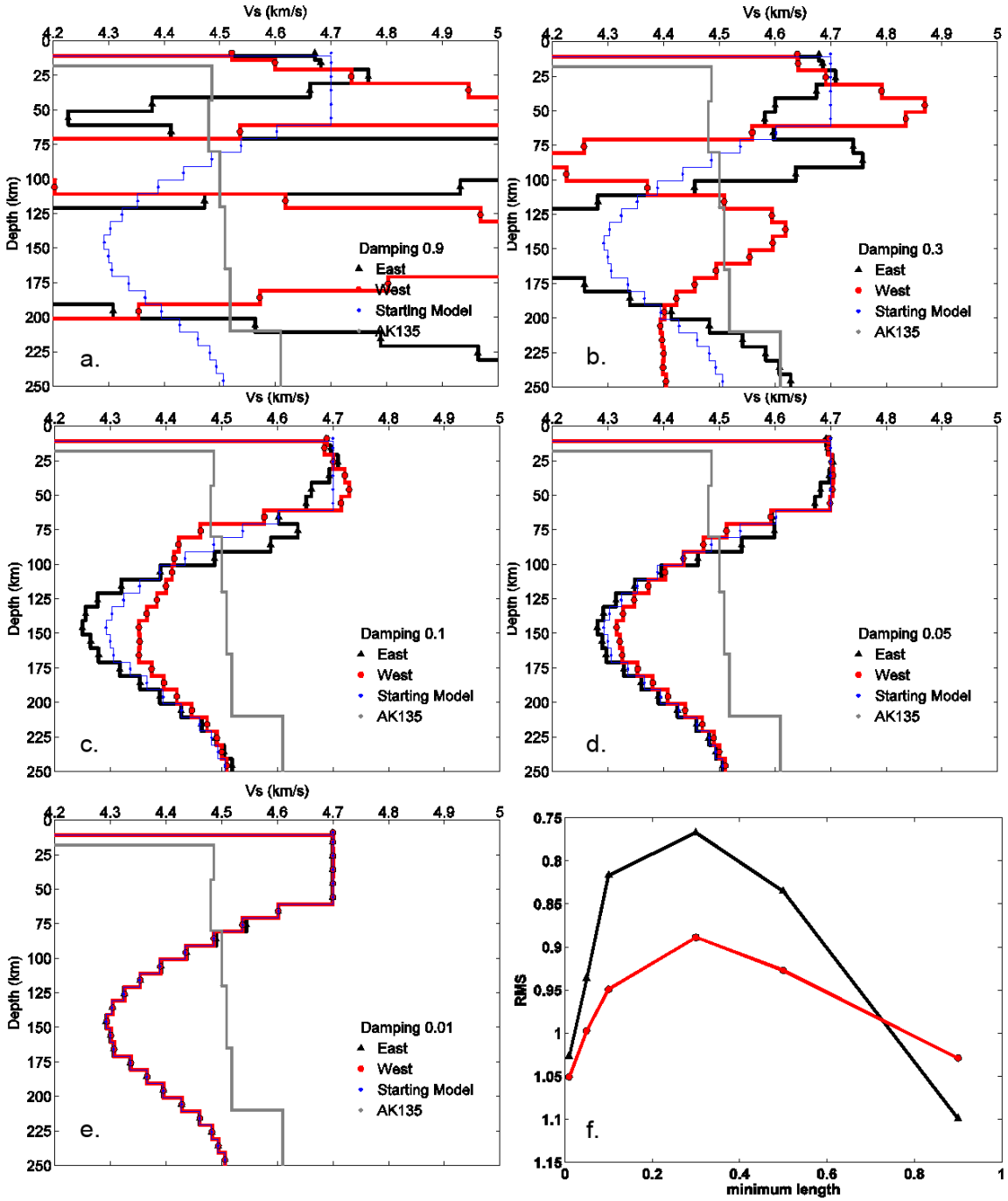

Figure 17. a-e) Results from tests run with inversion 2 and phase velocity data set P4. Red circles indicate the western region, black triangles the eastern region, blue dots the input Vs starting model, and the gray line the global Earth reference model AK135. Each window displays increased damping from 0.9 (a), 0.3 (b), 0.1 (c), 0.05 (d), to 0.01 (e). f) the trade-off curve between minimum length (model damping) and misfit calculated by equation (10).

Results from Figure 17 motivated me to conduct an in-depth investigation of the specifics of Inversion 2. I analyzed where in the inversion my final results are output into the file which is plotted, how many iterations are performed, and the variations of my starting model across layer depths, especially in the unstable shallow upper structure. To isolate where the issues are and how to best resolve them, I conduct three tests which question where the inversion outputs the optimal results, within the correct mathematic parameters, as shown in Figure 18. All three tests use the same starting model, input phase velocity set P4, same model damping parameter of 0.1 km/s, smoothing, curvature, and no data damping. The first test (Figure 18.a) removes an excessive and ineffective correctional factor applied by inversion 2 which does not exist in the original inversion 1. The second test (Figure 18.b) analyzes this additional correction by outputting the results only from the first iteration. The third test serves as the control for what how the inversion was initially written and run, which includes the correction factor inserted after an initial change is dictated by the inversion and is applied again to the input values (Figure 18.c). Results in Figure 18.b, Figure18.c have an additional small Low Velocity Zone (LVZ) in the east at 27 km depth which is unrealistic of this type of plate material and indicate that the additional correction is counterproductive. . The instabilities observed in these tests indicate that additional iterations are necessary to achieve the best fit in a least square sense. Looking at these tests that remove the correction, I find that it does not improve the fit to the data, nor is it necessary to produce stable results. Based on these findings, I designed a new procedure, inversion 3. Even though I test multiple variations for inversion 2, the test displayed in figure18.a is what is used to plot all results for the second inversion through all phase velocity data sets.

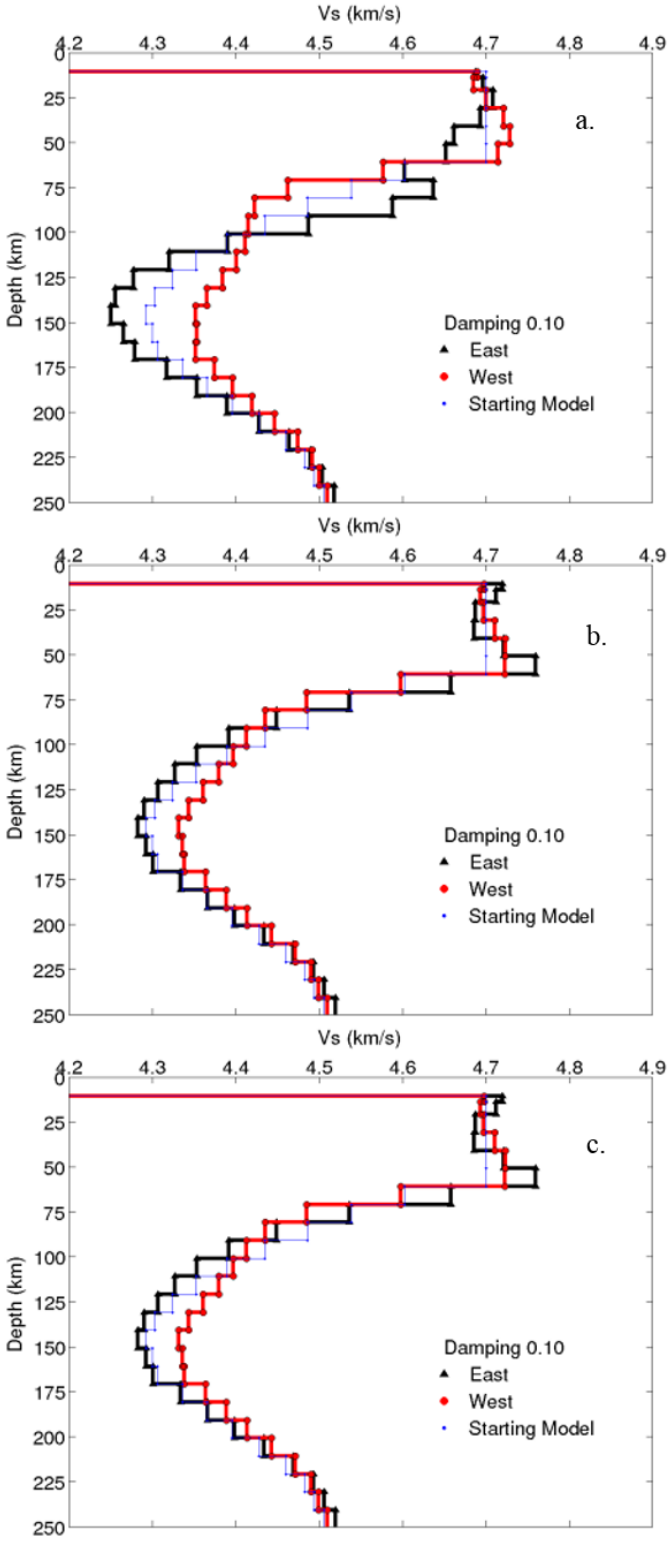

Figure 18. a) Test 1 removes an additional correctional factor, b) Test 2 outputs the results after 1 iteration, and c) Test 3 serves as the control for how previous results were run. Three slightly different tests run with inversion 2 and phase velocity data set P4.

Figure 19 shows the results from inversion 3 with phase velocity data set P4. The trade-off curve reveals that the results have converged (Figure 19.f), with the best fit identified at 0.1 km/s (Figure 19.c). With 10 iterations, the unstable western region results converge, and the eastern region is well resolved regardless of the applied damping parameters, since it is closely approximated by the starting model. The eastern region has a maximum velocity of 4.7 $\pm$ 0.06 km/s at 30 km $\pm$ 15 km, as seen in Figure 20. The velocity structure transitions into a negative velocity gradient extending to a minimum of 4.3 $\pm$ 0.08 km/s at 140 km $\pm$ 65 km depth. Within error, I am able to resolve four independent pieces of information about the area. 1) The low velocity zone can be as shallow as 35 km to 75 km depth; 2) it can extend as deep as 75 km to 125 km depth; and 3) it has a velocity range from 4.65 $\pm$ 0.07 km/s to 4.47 $\pm$ 0.08 km/s. To compare velocity structure results of my study area to global studies, velocities from a standard Earth model, AK135, 110+ Ma seafloor data (Nishimura and Forsyth, 1989) are plotted for reference. The PLATE velocity results are markedly higher than Nishimura and Forsyth, with a velocity difference of 2.15 % $\pm$ 1 % at 30 $\pm$ 15 km depth.

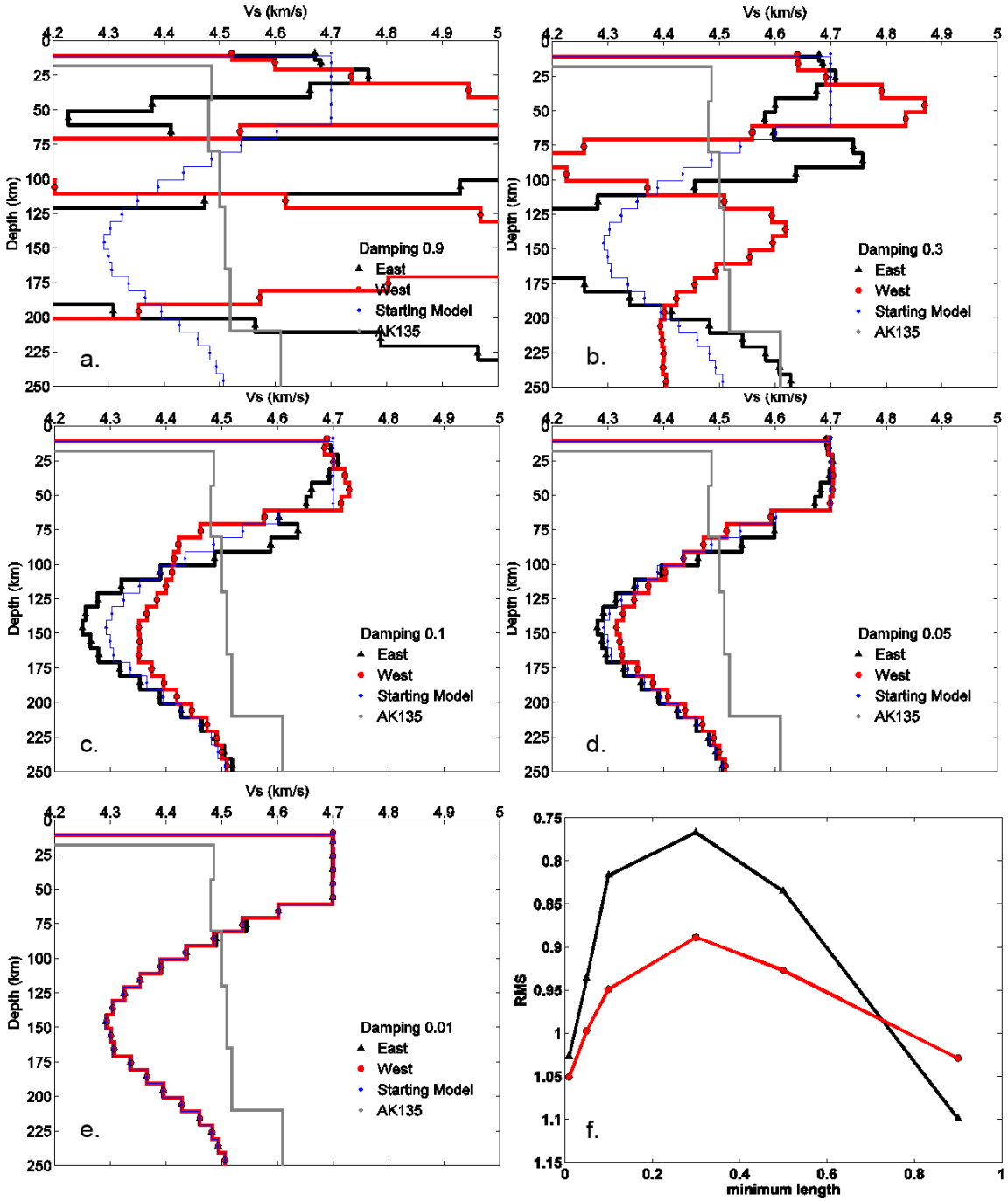

Figure 19. a-e) Results from tests run with inversion 3 and phase velocity data set P4. Red circles indicate the western region, black triangles the eastern region, blue dots the input Vs starting model, and the gray line the global Earth reference model AK135. Each window displays increased damping from 0.9 (a), 0.3 (b), 0.1 (c), 0.05 (d), to 0.01 (e). f) the trade-off curve between minimum length (model damping) and misfit calculated by equation (10).

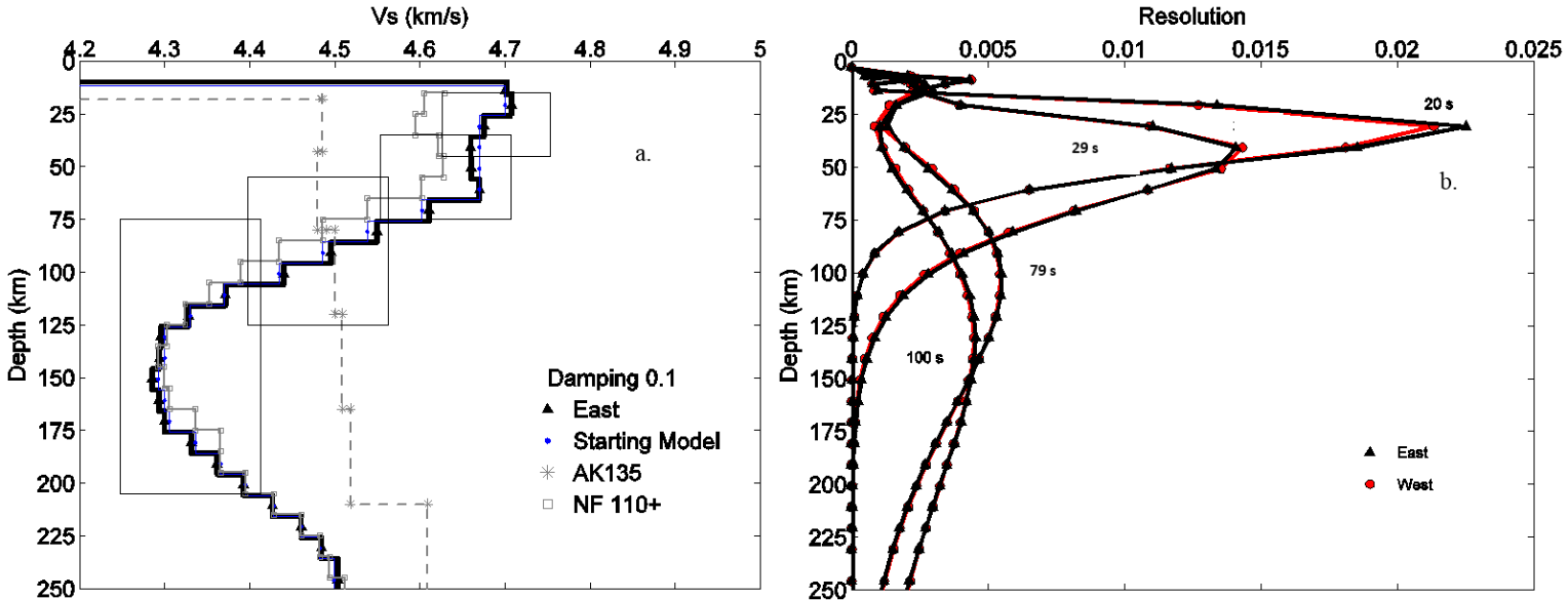

Figure 20. The final results chosen from Figure-inv3-P4-d. Black triangles indicate the final results, blue dots depict the input Vs starting model, gray squares are from previous studies of 110 + ma seafloor (Nishimura and Forsyth, 1989), and gray stars are from global reference Earth model AK135. The black boxes indicate both vertical and horizontal errors. Figure-sensitivity Resolution kernels for 20 s, 29 s, 79 s, and 125 s.

While the western region has less data coverage than the eastern region, resulting in higher error, I am still able to resolve four independent pieces of information within error, and extrapolate the velocity structure of the area (Figure 21). The velocities in the shallow upper structure at 30 $\pm$ 15 km depth are 3.21% faster than Nishimura and Forsyth (1989), though still within error, and 4.3 % faster than AK135. The western region velocities reach as high as 4.80 km/s $\pm$ 0.07 km/s. The region reaches a minimum of 4.33 km/s $\pm$ 0.10 km/s. The negative velocity gradient may be as shallow as 35 km to 75 km depth, or extend as deep as 75 km to 205 km depth. The negative velocity gradient is steeper in the western region than the eastern region, but has a smaller overall velocity change.

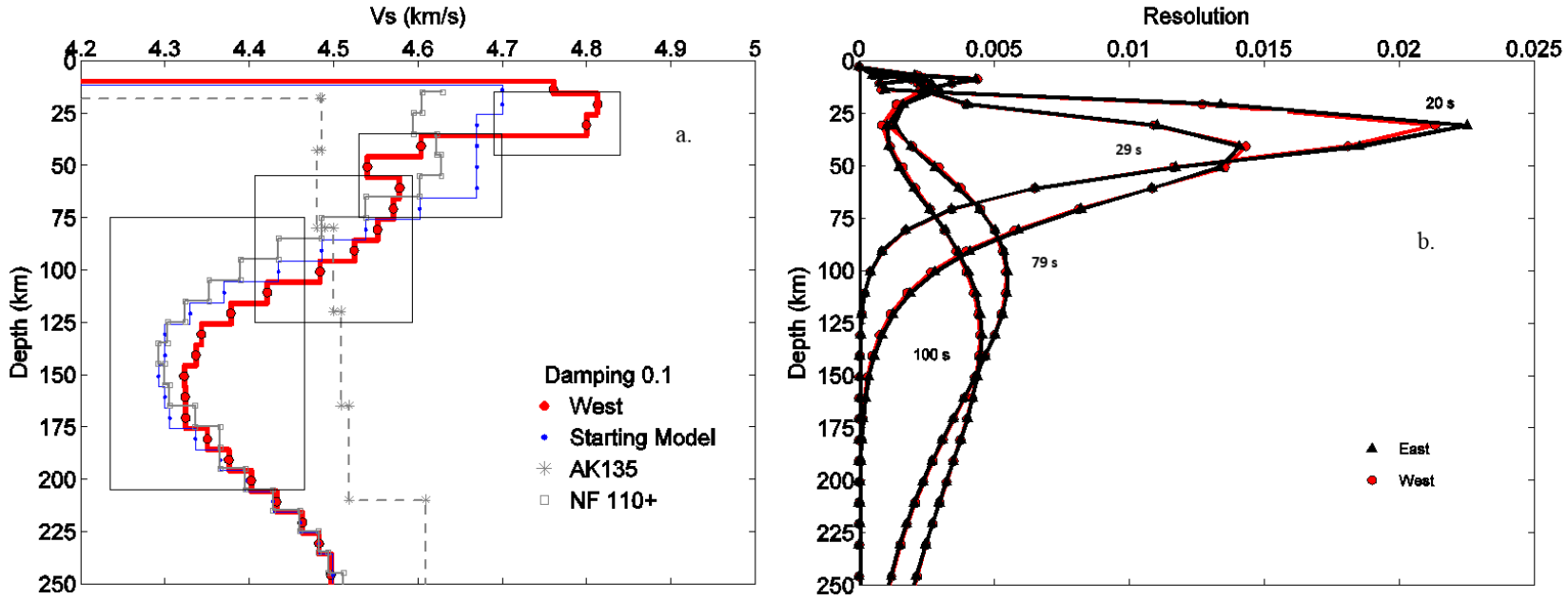

Figure 21. a)The final results chosen from Figure-inv3-P4-d. Red circles indicate the final results, blue dots depict the input Vs starting model, gray squares are from previous studies of 110 + ma seafloor (Nishimura and Forsyth, 1989), and gray stars are from global reference Earth model AK135. The black boxes indicate both vertical and horizontal errors. b) Figure-sensitivity Resolution kernels for 20 s, 29 s, 79 s, and 125 s.

To understand how well constrained these values are at various depths of importance, the resolution kernels for each region are plotted in Figure 22, as calculated by the partial derivatives of the phase velocity results with respect to shear wave velocity. Figure 22 shows that the regions slightly vary, with a mildly higher resolution peak depth of sensitivity in the eastern region. Based on my four independent pieces of information, I analyze the resolution for each of these depths in Figure-sensitivity. My four pieces of information at 15 km, 35 km, 100 km, and 150 km occur at approximately 20 s, 28 s, 79 s, and 125 s. The short period data at 20 s and 8 s are well resolved, with high resolution at 0.023 in the east, and 0.022 in the west. In the higher period data, the sensitivity peak drastically decreases to 0.006 in the east and 0.004 in the west. The resolution of the thickness of each depth layer is demonstrated by Figure-sensitivity. Data at 20s has best

sensitivity within a layer between 25-65 km, whereas data at 79 s is poorly constrained.

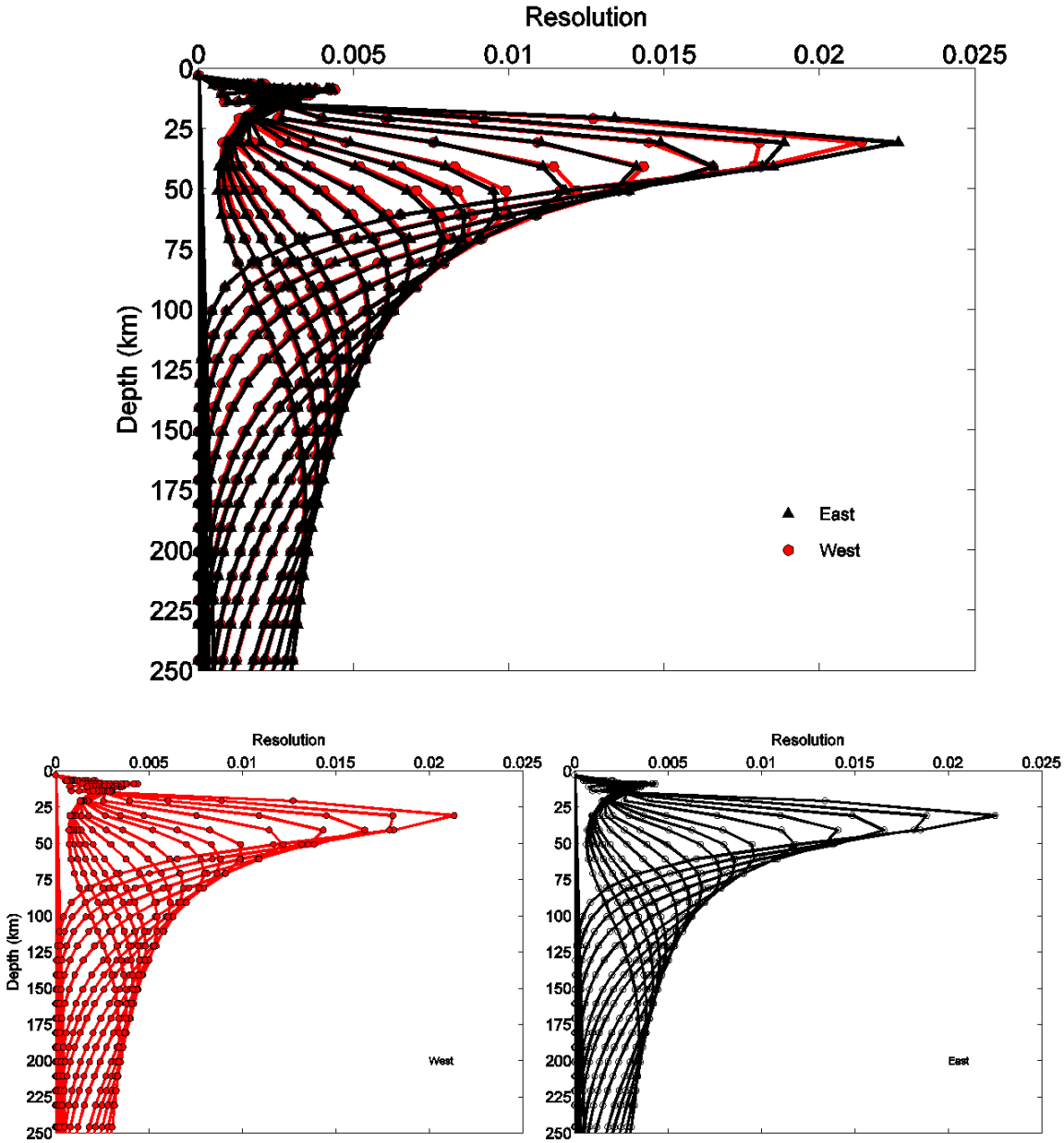

Figure 22. a) Sensitivity kernels for west (red curves) and east (black curves) regions, plotted t. Periods from 20 s to 143 s are shown. b) sensitivity kernels for the western and (red curves) c) eastern regions (black curves).

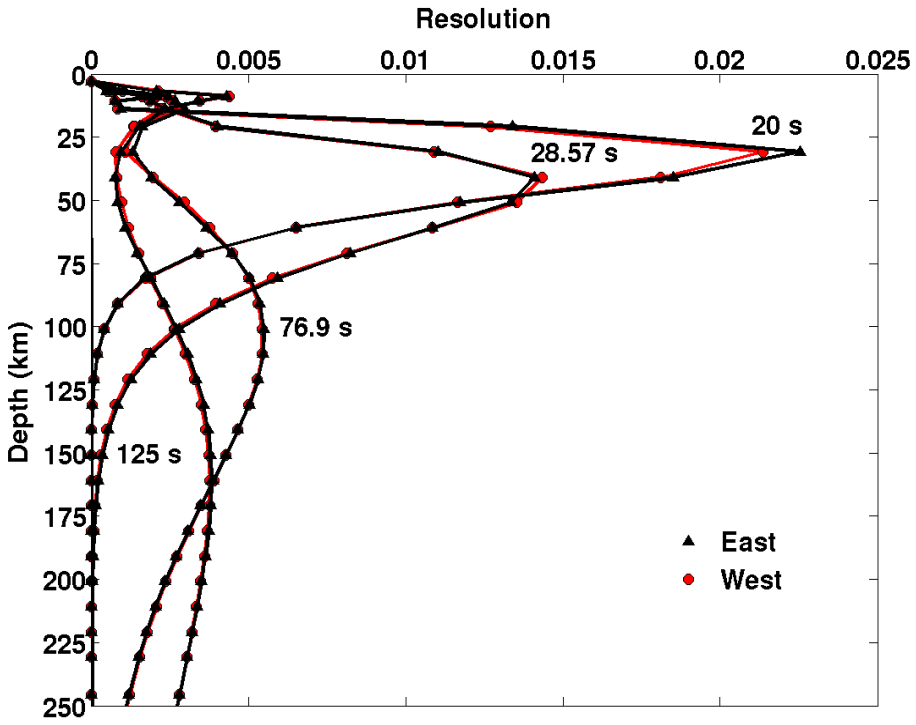

Figure 23. Resolution kernels for 20 s, 28.57 s, 76.9 s, and 125 s.

The thickness and peak depth of sensitivity, for each period, is described by the average wavelength for each period, and the partial derivatives of the related phase velocity with respect to shear wave velocity. Estimated average depth range of sensitivity for periods from 18 s to 143 s range from 70 km to 613 km, but the peak depth of sensitivity range is smaller, from 24 km to 190 km. The sensitivity kernels indicate that while the model is robust at shallow depths where high velocities are seen, deeper depths of interest are less resolved.

Chapter 5

Discussion

I observe extremely high velocities for my study area of 150-160 Ma seafloor. With velocities up to 4.8 km/s in the shallow structure, these are some of the highest recorded shear wave seismic velocities seen anywhere in oceanic lithosphere. I define the LAB by the depth at the middle of the negative velocity gradient below this highest velocity. The eastern region indicates the LAB is at 90 km $\pm$ 35 km depth, whereas the western region displays an LAB at 80 km $\pm$ 45 km depth. While the eastern and western regions appear to have slightly different maximum and minimum velocities, as well as a varied lithospheric thickness, the two regions are approximately the same within error. In the shallow upper structure of my study area, at approximately 30 km, velocities are 2 % higher in the East and 3% higher in the West within error as compared to (Nishimura and Forsyth, 1989) for 110 + Ma data (Figure 20, Figure 21). Few studies are available on seafloor age over 100 Ma. S receiver techniques used on Pacific seafloor beneath Japan (Kumar and Kawakatsu et al., 2011) at 130 Ma indicate that the LAB occurs at 74.1 km $\pm$ 5.6 km depth, which is consistent with the LAB depth I report here. Previous studies using ScS phases in 100 Ma seafloor (Gaherty et al., 1999) have the same velocities observed in my PLATE study (Figure 24) but with a shallower LAB. The difference in depth indicates only about 20-30 km thickening of the lithosphere over the last 50 Myr.

Rayleigh wave inversion studies performed on 5-9 Ma seafloor in the East Pacific Ocean report maximum velocities of 4.4 km/s from the GLIMPSE project (Yang et al., 2007) and a LAB of 40 km depth (Figure 24; Weeraratne et al., 2007). Seafloor magnetotelluric data indicate the LAB is defined by a dehydration boundary which is resistive above the LAB and conductive below (Evan et al. 2006). Magnetotelluric data also imply a mantle thickness of 60 km in 2 Ma seafloor near the East Pacific Rise (MELT project; Kiyoshi and Pascal et al., 2006).

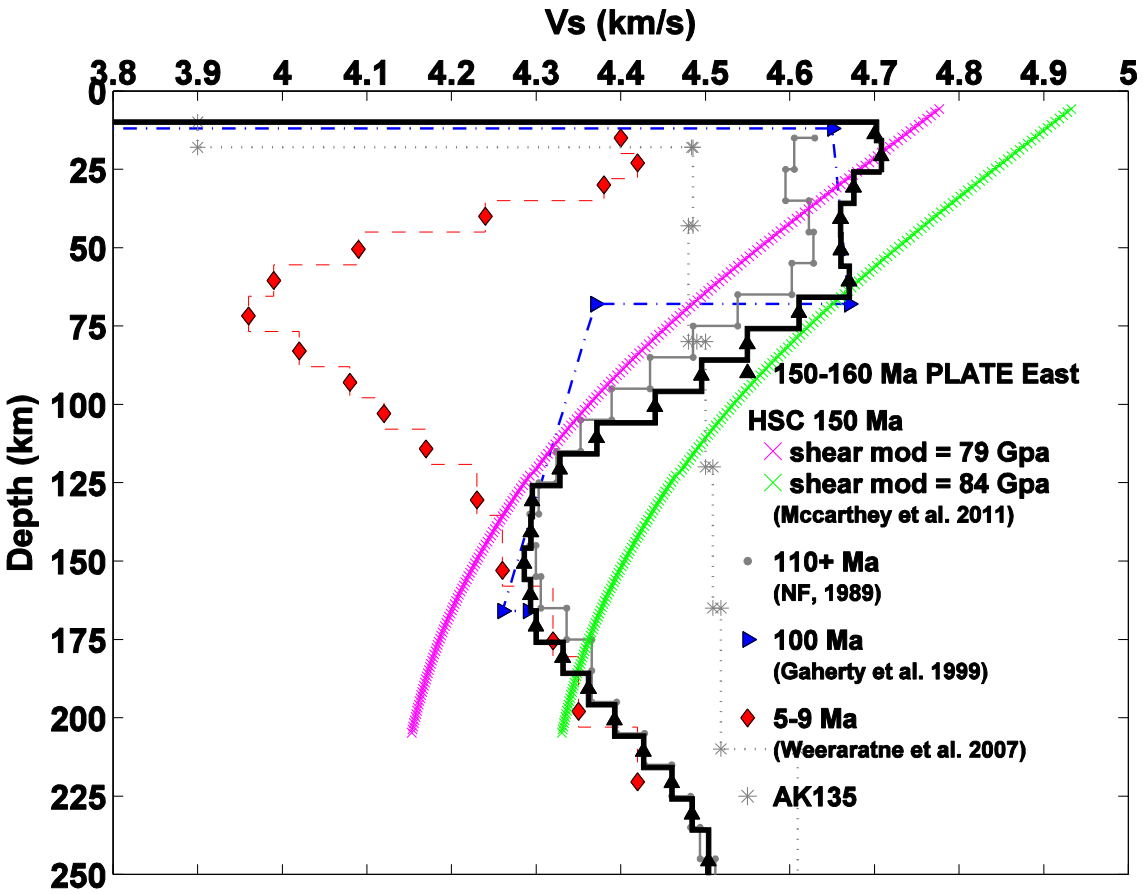

Figure 24. A comparison of a variety of oceanic shear wave velocities from previous studies with PLATE shear wave velocities from the eastern region (Figure 20). Black triangles represent PLATE velocities in the eastern region. Gray stars depict the global reference model AK135. Gray squares are from global land station receiver functions placed along the Pacific plate for 110 + Ma seafloor (Nishimura and Forsyth, 1989). Blue right facing triangles are 100 Ma seafloor (Gaherty et al., 1999) and red diamonds are from young 5-9 Ma seafloor off the Eastern Pacific plate (Weeraratne et al., 2007). Pink and green lines indicate half space cooling velocity structure predictions for shear modulus values which fit within my error (Faul and Jackson, 2005; McCarthey et al., 2011).

Petrologic studies that approximate grain size and shear modulus in 100 Ma Pacific seafloor report velocities of 4.8 km/s and above (Fault and Jackson, 2005). Analysis of shear modulus and strain dissipation with respect to period and the chosen isotherm indicate that as temperature increases, shear modulus decreases (McCarthey et al., 2011). Dehydration of peridotite should increase shear modulus, as well as minutely increase density, making old dehydrated mantle resistant to shear. The variation of shear modulus is further dependent on the specified isotherm. The previously discussed GDH1 model (Stein and Stein, 1992) suggests that the lithosphere for sufficiently old seafloor is

hotter and deeper than the HSC model, with a isotherm of 1950 °C and slower peak velocities of approximately 4.6 km/s, along with a LAB location at 95 km depth.

These shear wave velocity studies highlight the importance of estimating the appropriate isothermal gradient for the study area in question. Half-space conductive cooling model in a semi-infinite half-space is dependent on age as well as the approximated isothermal boundaries. Figure 4 explores the approximated LAB depth for a range of isotherms based on Equation (1). Velocity structure approximated by the half space cooling model (Fault and Jackson, 2005; McCarthey et al., 2011), which is strongly dependent on shear modulus, indicates that only shear modulus values between 79 and 84 GPa fit my PLATE velocities within error. This result suggests that the half space cooling model is sufficient to explain my observations. However, this does not rule out alternate models for thinner lithosphere given my errors in Figure 20 and 21.The Plate model (e.g. Doin and Flout, 1996) stops accounting for seafloor subsidence at 80 Ma, after which the model reaches an asymptote regardless of the selected isotherm, and becomes solely dependent on the chosen isotherm. By stacking SS waveforms using 17 years of Pacific Ocean lithosphere data, a study of isothermal effects on plate thickness suggest that old seafloor (> 70 Ma) has a distinct thermal boundary at 950 °C, and may indicate the boundary is a permeability layer responsible for the lithospheric thinning which deviates from the half-space conductive cooling model (Rychert et al., 2011). Calculations which isolate the conductive part of the isotherm until it intersects with the isentropic profile for a given isotherm predict lithospheric depth in a previous studies (McKenzie and Priestly, 2005; 2006). These results claim that the accuracy of temperature constraints increases with depth, with a distinct accuracy boundary at temperatures greater than 1100 °C at 110 + km depth. Thermal modeling of half space cooling (Faul and Jackson, 2005; McCarthey et al., 2011), which gives velocity structure (Figure 24), indicates that the HSC velocity structure is similar to results for the PLATE project. To better constrain this result, additional petrologic studies are needed to resolve whether the lithosphere may be a simple solid slab which evolves along a single isotherm, or if the plate thickness and density are affected by isothermal variations approximated by additional dynamic sources other than simple conductive cooling.

To further constrain whether this simple growth model is effective, PLATE results are compared to continental studies (Figure 25). The PLATE project results, indicates high velocities at 4.8 km/s.

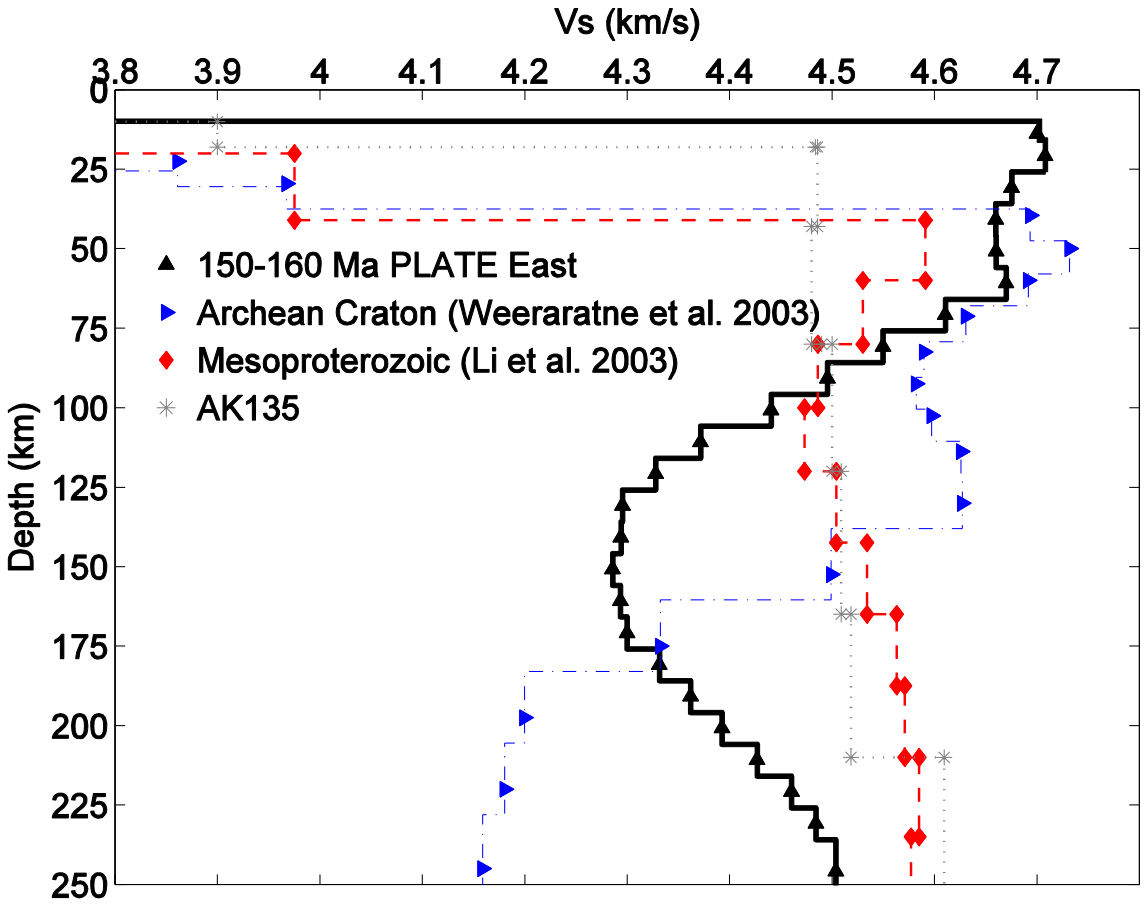

Figure 25. A comparison of a variety of continental shear wave velocities from previous studies with PLATE shear wave velocities from the eastern region (Figure-moneyshot-east). Black triangles represent PLATE velocities in the eastern region. Gray stars depict the global reference model AK135. Blue right facing triangles are from Archean craton in Tanzania (i.e. 2,000 Ma; (Weeraratne et al., 2003). Red diamonds are from Mesoproterozoic continental crust in Eastern North America plate (Li et al., 2003).

Seismic velocity datasets from several studies in different areas are shown in Figure 25. Comparison of PLATE velocity structure to normal continental Mesoproterozoic lithosphere in the Eastern North America plate display markedly lower velocities, reaching a maximum of 4.6 km/s. The North America plate indicates only a 2.6% difference between the maximum lithospheric velocity structure and the minimum in the LVZ. The depth of the LAB at 60 – 70 km is slightly shallower than the PLATE LAB. Examining the velocities in continental Archean cratonic regions provides an interesting

comparison with my results (Figure 25). Most notably, maximum velocity results of 4.74 km/s in upper 75 km of the Tanzanian lithosphere is identical within error for 150-160 Ma oceanic lithosphere in my study area. The Archean craton velocity structure is complex and demonstrates a mid-lithosphere discontinuity at 75 km, below which velocities drop to 4.6 km/s. Velocities in the Archean craton lower lithosphere and maximum values in the upper lithosphere of Mesoproterozoic oceanic lithosphere are the same (at least in this one location). This may suggest that they formed by a similar process of subduction-related re-working in an arc wedge setting for over 2,000 Ma. This similarity may indicate that the upper lithosphere of continental plates is not significantly modified by plate tectonic activity over time. Studies suggest that peridotite depletion of the upper mantle controls continental evolution and stability (Jordan et al. 1998). Depleted peridotite is resistant to reintegration into the undepleted mantle. As previously suggested, shear modulus stabilizes at lower temperatures, meaning that plate motion and horizontal shear strain will only occur deeper in the Earth where temperatures are high enough depths. These properties help differentiate between crust, thermal anomalies, and mass motion propelled by small scale convection. Alternate hypotheses say this discontinuity may be caused by small volumes of partial melt or hydration in the lower lithosphere below a dehydrated upper lithosphere (Rychert et al., 2011).

My suggestion for a simple formation history is consistent with observations of anisotropy in previous studies (Sotirov, 2014), which show a single anisotropic fabric at periods below 80 s in both the eastern and western region consistent with the magnetic anomalies in each area respectively (Figure 26). The only change in anisotropy is observed at sublithospheric depths associated with active asthenospheric flow. Since my study area was specifically conducted along a magnetic bight, I am able to compare anisotropy recorded by the magnetic bight. While remnant anisotropy frozen into the upper lithosphere should be parallel to Pacific plate motion in the western region, remnant anisotropy should be perpendicular to plate motion in the eastern region (Figure 26). The anisotropy resultant from the phase velocity inversion indicates velocities that are 1.3% higher than predicted along with a lithospheric thickness of 60 km (Sotirov, 2014).

The high velocities seen in my results, indicate that oceanic lithospheric growth is a simple, single layer process. Since velocities in old Pacific seafloor are similar to Archean cratons, they may share physical properties that affect seismic velocity such as density, temperature, or dehydration. The oceanic plate must be sufficiently cold, dense, or dehydrated to accommodate such high velocities. While results are dependent on the chosen isotherm at the base of the lithosphere, the requirements of the observed data remain proportionally intact with markedly high velocities.

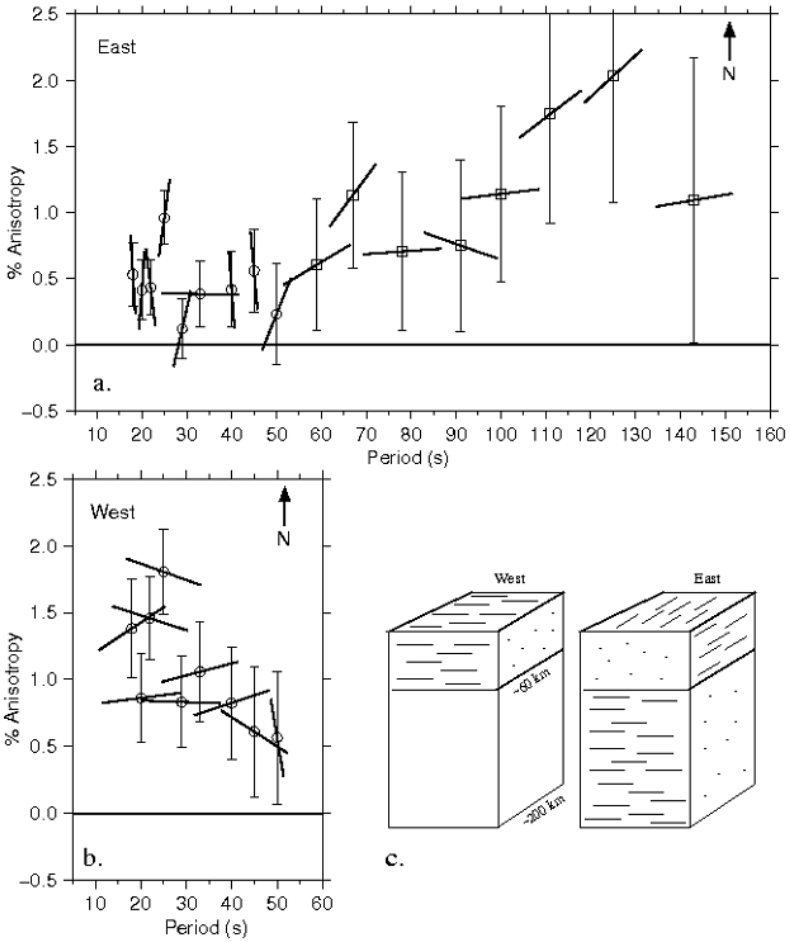

Figure 26. Anisotropy (Sotirov, 2014) direction and magnitude over the eastern a.) and the western region (east of 152º longitude). Position of the circles indicates the magnitude of the anisotropy in percentile at each period. Squares indicate that the usage of the single plane wave method. The vertical error bars indicate the error in magnitude in 1σ. The direction of the anisotropy relevant to north at each period is indicated by the direction of the thick black line. c.) Schematic of anisotropy as function of depth.

The minimum LVZ seen in PLATE is 2 % higher than the minimum LVZ seen in Archean craton (Figure 20, Figure 25). While it is unknown what causes restricted growth of the lithosphere in the PLATE study area, tomographic studies from the Eastern

African Archean craton indicate a large mantle plume (super plume) rises from the core-mantle boundary (Nyblade, 2002; Ritsema et al., 2000). The similarity in low velocities in the two studies is surprising and may indicate a dynamic source of long distance flow in asthenospheric channels from a plume source (e.g. the Hawaiian plume) to the PLATE study area if alternative models for lithospheric thinning are considered. Models for long distance flow such as small scale convection (Korenga and Jordan, 2003) or viscous fingering through the asthenosphere (Weeraratne et al., submitted 2015) may be valid models to explain plate growth behavior if half space cooling is insufficient. Scaling of the viscous fingering model to the Earth's upper mantle indicates that the ratio of asthenospheric thickness (B) to the propagation distance of fingering (L) is large, B/L > 30 (Nissanka, 2014). Assuming an asthenospheric thickness in my study area of ~130 km (Figure 20), dynamic fingering structures in the presence of overriding plate motion may travel over 4,000 km downstream from a plume source, consistent with the distance of my PLATE study area from sources such as the Hawaiian plume. The Hawaiian Islands reside on seafloor that is approximately 80-120 Ma. If an upwelling plume were affecting this region, it would limit lithospheric cooling and growth compared to the HSC model. Since this lithosphere would be warmer than predicted by the HSC, we would expect less subsidence than predicted by the HSC for all areas affected by the plume. The PLATE study area is 4,000 km from the plume, and shows signatures of being affected by it. All the material between the plume and the PLATE site would also be affected. Ultimately, my limited results within error results in two possible scenarios: 1) no plate thickening has occurred over the last 50 My and conductive cooling is not effective or 2) significant thickening of 20 – 50 km has occurred over the last 50 My and conductive cooling is sufficient and is still occurring.

Chapter 6

Conclusion

By performing a Rayleigh wave inversion for shear velocities in the Northwestern Pacific Oceanic on OBS PLATE data, I am able to better-describe oceanic plate formation and growth up to very old ages. Similar previous studies are limited to 110 Ma and younger, and were inhibited by the technically challenging nature of data collection, and associated expensive budgeting, which made marine seismic research prohibitive. Shear wave velocity results observed in 150-160 Ma Northwest Pacific seafloor are markedly higher than previous studies (Nishimura and Forsyth, 1989), reaching up to 4.8 km/s $\pm$ 0.09 km/s, which is up to 2-3% greater than alternate studies within error in the upper lithosphere. The PLATE project shear wave velocity structure displays a strong negative velocity gradient with indicates a LAB depth of 90 km $\pm$ 35 km. The Eastern and Western regions are near- identical within error. The half-space conductive cooling model (Parsons and Sclater, 1977) with an assumed isotherm of 1350 °C predicts a plate thickness in 150-160 Ma seafloor is similar within my error. These velocities are remarkable because they resemble velocities seen in previous studies on 100 Ma Pacific seafloor (Gaherty et al., 1999). This study also indicates a LAB at 68 km depth which may be thinner than indicated for my PLATE study area at 150 Ma seafloor, but is not significant within error. When compared with PLATE data, only 20-30 km of plate thickening have taken place over 50 My, and plate velocities remain the same over this period. Rayleigh wave inversion studies on 5-9 Ma seafloor in the Eastern Pacific Ocean report maximum velocities of 4.4 km/s from the GLIMPSE project (Yang et al., 2007) and a LAB of 40 km depth (Weeraratne et al., 2007), which is significantly thinner than LAB depths I report here suggesting growth with age. However, my results are similar to HSC predictions when shear modulus is limited to 79 – 84 GPa within my error.

I am also able to compare the PLATE data to continental lithosphere previous studies. When plotted with data from Mesoproterozoic crust age shear wave data (Li et al., 2003) and East African Archean Craton (Weeraratne et al., 2003), PLATE velocities are extremely similar in the upper lithosphere. Mesoproterozoic crust velocity structure indicates a subtle velocity contrast of only 4% difference between the maximum and

minimum velocities. The resemblance of velocities in Archean craton and 150-160 Ma oceanic seafloor may help to understand how both oceanic and continental plates evolve with time. Continental plates are a complex, multi-layer growth process where the upper lithosphere is not significantly modified by plate tectonic activity over time. Relative to this, oceanic lithosphere is a simple- single layer structure over a single LVZ which grows and cools with time and is sufficiently described by half space cooling. A model of simple oceanic plate formation history is consistent with anisotropy observations in previous studies (Sotirov, 2014), which indicates a single anisotropic fabric at periods below 80 s.

The observed high velocities in the lithosphere eliminate the presence of partial melt in the same area, however it may be present at the LAB discontinuity, where a dehydrated upper lithosphere is formed over a hydrated lower lithosphere (Rychert et al., 2011). The similarity between mantle plume source Archean craton velocities and oceanic PLATE velocities may suggest a dynamic source of long distance plume- related flow. However, within my relatively large errors, concrete suggestions cannot be made as to whether half space conductive cooling is the sole and/or partially effective method of lithospheric growth, suggesting better seismic data sets in old seafloor are necessary.

References

Booth,C.M., D.W. Forsyth and D. S. Weeraratne, 2014, Upper mantle Q structure beneath old seafloor in the western Pacific,*Journal of Geophysical Research: Solid Earth* Volume 119, Issue 4, April 2014, pp. 3448–3461,DOI: 10.1002/2013JB010589, 2014.

Doin, M.P., and F. Fleitout, Thermal evolution of the oceanic lithosphere: an alternative view, Earth and Planetary Science Letters, 142, 121-136, doi: ,1996.

Evans, R. L., G. Hirth, K. Baba, D. Forsyth, A. Chave, and R. Mackie (2005), Geophysical evidence from the MLET area for compositional controls on oceanic plates, *Nature*, 437,249-252.

Faul, U.H., Jackson, I., The seismological signature of temperature and grain size variations in the upper mantle, Earth and Planetary Science Letters, 234, 119-134, 2005.

Forsyth, D. W., and Li, A., Aray analysis of two-dimensional variations in surface wave phase velocity and azimuthal anisotropy in the presence of multipathing interference, AGU, vol . 157, 81- end, 2005.

Gaherty, J.B., Seismological structure of the upper mantle: a regional comparison of seismic layering, Earth and Planetary Sciences, 110, 21-41, 1999.

Huang, J., and S. Zhong, Sublithospheric small-scale convection and its implications for the residual topography at old ocean basins and the plate model, J. Geophys. Res., 110, B05404, doi:10.1029/2004JB003153, 2005.

Jordan, T.H. (1978). Composition and development of the continental tectosphere. *Nature*, 74(5671),544-548.

Karato, S., and H. Jung (1998), Water, partial melting and the origin of the seismic low velocity and high attenuation zone in the upper mantle, *Earth Planet. Sci. Lett.,157* 193-207.

Kiyoshi B., P. Tarits, A.D. Chave, R.L. Evans, G. Hirth, and R.L. Mackie (2006), Electrical structure beneath the northern MELT line on the East Pacific Rise at 15°45'S, J. Geophys. Res, 33,L2301,doi:10:1029/2006GL027528,2006.

Korenga, J., Jordan, T.H., Physics of multiscale convection in Earth's mantle: Onset of sublithospheric convection, J. of Geophys. Res., Vol. 108, 2003.

Kumar, P. and Kawakatsu, H., Imaging the seismic lithosphere-asthenosphere boundary of the oceanic plate, G3, Vol. 12, 2011.

Li, A., D. W. Forsyth and K. M. Fischer, Shear velocity structure and azimuthal anisotropy beneath eastern North America from Rayleigh wave inversion, J. Geophys. Res., 108, B8, 2362, 10.1029/2002JB002259, 2003.

McKenzie, D. P., Some remarks on heat flow and gravity anomalies, Journal of Geophysical Research, 72, 6261-6273, 1967.

McKenzie, D., Jacksons J., and Priestley, K. Thermals structure of oceanic and continental lithosphere, Earth and Planetary Science, 233, 337-339, 2005.

Nishimura, C.E., and D.W. Forsyth, The anisotropic structure in the upper mantle of the Pacific, Geophys. J., 96, 203-229, 1989.

Nyblade, A.A., Crust and upper mantle structure in East Africa: implications for the origin of Cenozoic rifting and volcanism and the formation of magmatic rifted margins, *Volcanic Rifted Margins,* edited by M.A. Menzies et al., *Spec. Pap. Geol. Soc. Am., 362,* 15-26, 2002.

Oikawa, M., Kentaro, K., and A. Nishizawa, Seismic structures of 154-160 Ma oceanic crust and uppermost mantle in the Northwest Pacific Basin, Earth Planets Space, 62, e13-e16, doi:10.5047/eps. 2010.

Parsons, B., and J.G. Sclater, An analysis of the variation of ocean floor bathymetry and heat flow with age, J. Geophys. Res., 82, 903-827, 1977.

Priestley, K., and D. McKenzie, The thermal structure of the lithosphere from shear wave velocities, Earth Planet. Sci. Lett., 244, 285-301, 2006.

Richter, F. M., and B. Parsons (1975), On the interaction of two scales of convection in the mantle, J. Geophys. Res., 80, 2529-2541.

Ritsema, J., A. A. Nyblade, T.J. Owens, C. A. Langston, and J.C. VanDecar, Uer mantle seismic velocity structure beneath Tanzania, East Africa: Implications for the stability of cratonic lithosphere, J. Geohys. Res., 103, 21, 201-21,213,1998.

Ritzwoller, M. H., Shapiro, M. H., and S. Zhong, Cooling history of the Pacific lithosphere, Earth and Planetary Science Letters, 226,69-184, doi: 10.1016/j.epsl, 2004.

Rychert, C.A., and P. M. Shearer (2011), Imaging the lithosphere-asthenosphere boundary beneath the Pacific using SS waveform modeling, *J. Geophys. Res., 116*, B07307, doi:10.10292010JB0087070.

Saito, M. (1988), DISPER80: A subroutine package for the calculation of seismic normal-mode solutions, in *Seismological Algorithms*, edited by D.J. Doornbos, 293-319, Elsevier, New York.

Simon, N. S. C., E.R. Neumann, C. Bonadiman, M. Coltorti, G. Delpeche, M. Gregoire, and E. Widom (2008), Ultra-refractory Domains in the Oceanic Mantle Lithosphere Sampled as Mantle Xenoliths at Ocean Islands,J. of Petrology, 49, 6, 1223-1251 2008, doi:10.1093/petrology/egn023.

Shinohara, M., T. Fukano, T. Kanazawa, E. Araki, K. Suyehiro, M. Mochizuki, K. Nakahigashi, T. Yamada, K. Mochizuki (2008) Upper mantle and crustal seismic structure beneath the Northern Pacific Basin using a seafloor borehole broadband seismometer and ocean bottom seismometers, Physics of Earth and Planetary Interiors,170,95-106,doi:10.1016/j.pepi2008.07.039.

Shintaku, N., D.W. Forsyth, C.J. Hajewski, and D.S. Weeraratne (2014), Pn anisotropy in Mesozoic western Pacific lithosphere, J. Geophys. Res. Solid Earth, 119, 3050-3063, doi:10.1002/2013JB010534.

Sotirov, T. (2014), Rayleigh wave phase velocities and anisotropy of old oceanic lithosphere in the Pacific (Master's Thesis).

Stein, C.A., and S. Stein, A model for the global variation in oceanic depth and heat flow with lithospheric age, Nature, 359, 123-129, doi:10.1038/35912a0, 1992.

Stixrude, L., and C. Lithgow-Bertelloni (2005), Mineralogy and elasticity of the oceanic upper mantle, origin of the low-velocity zone, J. Geophys. Res., 110, B03204,doi:10.1029/2004JB002965.

Takeo, A., Nishida, K., Isse, T., Kawakatsu, H., Shiobara, H., Sugioka, H., and T. Kanazawa, Radially anisotropic structure beneath the Shikoku Basin from broadband surface wave analysis of ocean bottom seismometer records, J. of Geophys, doi: 10.1029. 2013.

Walter, M.J.,(1998), Melting of garnet peridotite and the origin of komatiite and depleted lithosphere, J. of Petrology, 39, 1, 29-60.

Weeraratne, D.S., E.M.Parmentier, U. Nissanka, Viscous fingering in the oceanic and continental asthenosphere, EPSL, to be submitted 2015.

Weeraratne, D. S., D. W. Forsyth, Y. Yang, and S. C. Webb, Rayleigh wave tomography beneath intraplate volcanic ridges in the South Pacific, J. Geophys. Res., 112, B06303, doi:10.1029/2006JB004403, 2007.

Weeraratne, D. S., D. W. Forsyth, K. M. Fischer, A. A. Nyblade, Evidence for an upper mantle plume beneath the Tanzanian craton from Rayleigh wave tomography, J. Geophys. Res.,108,2427,doi:10.1029/2002JB002273,2003.

Yang, Y., and D. W. Forsyth (2006), Rayleigh wave phase velocities, small-scale convection, and azimuthal anisotropy beneath southern California, J. Geophys. Res. 111, B07306, doi: 10.1029/2005JB004180.

Appendix A. Input starting Model

Depth	Density	Vp(km/s	Vs(km/s)
5.80	1.0300	1.5000	0.0000
2.00	2.3000	4.3000	2.0000
2.00	2.8000	6.4000	3.5000
2.00	3.1000	6.9000	3.8000
4.00	3.3819	8.1500	4.7000
10.00	3.3900	8.1500	4.7000
10.00	3.3819	8.1500	4.6700
10.00	3.3669	8.1500	4.6700
10.00	3.3530	8.1500	4.6700
10.00	3.3583	8.1500	4.6700
10.00	3.3583	7.9996	4.6022
10.00	3.3614	7.8640	4.5381
10.00	3.3650	7.7670	4.4856
10.00	3.3676	7.6848	4.4345
10.00	3.3702	7.6178	4.3700
10.00	3.3727	7.5688	4.3300
10.00	3.3754	7.5358	4.3000
10.00	3.3754	7.5188	4.3000
10.00	3.3754	7.5228	4.2923
10.00	3.3754	7.5618	4.2997
10.00	3.3811	7.6018	4.3056
10.00	3.3811	7.6859	4.3361
10.00	3.3893	7.7709	4.3655
10.00	3.3893	7.8569	4.3951
10.00	3.3946	7.9469	4.4280
10.00	3.3946	8.0379	4.4603
10.00	3.4087	8.1069	4.4823
20.00	3.4087	8.1549	4.4990
20.00	3.4234	8.2390	4.5100
20.00	3.4533	8.2650	4.5000
20.00	3.4533	8.3140	4.5142
20.00	3.4560	8.3870	4.5402
20.00	3.4560	8.5260	4.6084
20.00	3.4860	8.6940	4.6840
20.00	3.4860	8.8800	4.7770

Appendix B. Shear Wave Velocity Results

East

Depth	Vs	Vs error	Depth error
2.9000001	0		
6.80000019	1.999114671		
8.80000019	3.49831146		
10.8000002	3.798834691		
13.8000002	4.702085343		
20.7999992	4.707859443	0.0635 km/s	30 km
30.7999992	4.675182793		
40.7999992	4.659745819		
50.7999992	4.660093566	0.0770 km/s	40 km
60.7999992	4.669767652		
70.8000031	4.610492874	0.0824 km/s	70 km
80.8000031	4.549464323		
90.8000031	4.495316361		
100.800003	4.440225888		
110.800003	4.371375562		
120.800003	4.327741384		
130.800003	4.295205672		
140.800003	4.293762361	0.0824 km/s	130 km
150.800003	4.285535483		
160.800003	4.293113934		
170.800003	4.299693056		
180.800003	4.331193094		
190.800003	4.361753751		
200.800003	4.392555249		
210.800003	4.426664702		
220.800003	4.46031925		
230.800003	4.484180124		
245.800003	4.503546425		

West

Depth	Vs	Vs error	Depth error
2.9000001	0		
6.80000019	2.013491		
8.80000019	3.525811		
10.8000002	3.834299		
13.8000002	4.760957		
20.7999992	4.813011	0.0749 km/s	30 km
30.7999992	4.799902		
40.7999992	4.603604		
50.7999992	4.540111	0.0849 km/s	40 km
60.7999992	4.578173		
70.8000031	4.570787	0.0932 km/s	70 km
80.8000031	4.552107		
90.8000031	4.524661		
100.800003	4.483938		
110.800003	4.421242		
120.800003	4.378342		
130.800003	4.343059		
140.800003	4.336763	0.1151 km/s	130 km
150.800003	4.322668		
160.800003	4.324033		
170.800003	4.324509		
180.800003	4.350293		
190.800003	4.375732		
200.800003	4.402106		
210.800003	4.432433		
220.800003	4.462633		
230.800003	4.482638		
245.800003	4.497007		

Appendix C. Inversion Tables

	Inv. Type	Phvel Input	Shvel Input	Data Damping	Model Damping	Min Curvature	Min length	RMS
1	1	Ao	NF 110+	None	0.2	n/a	0.2	n/a
2	1	A0	NF 110+	None	0.2	n/a	0.2	n/a
3	1	Ao	4.7 km/s	None	0.2	n/a	0.2	n/a
4	1	A	4.7 kms	None	0.2	n/a	0.2	n/a
5	1	A	4.65 kms	None	0.2	n/a	0.2	n/a
6	1	A	4.6 km/s	None	0.2	n/a	0.2	n/a
7	2	A	4.7 kms	2	yes	1	1.5	2.612
8	2	A	4.7 km/s	2	yes	1	1.1	2.612
9	2	A	4.7 km/s	2	yes	1	0.9	2.612
10	2	A	4.7 km/s	2	yes	1	0.5	1.508
11	2	A	4.7 km/s	2	yes	1	0.3	2.612
12	2	A	4.7 km/s	2	yes	1	0.1	2.612
13	2	A	4.7 km/s	2	Yes	1	0.05	1.34
14	2	A	4.7 km/s	2	Yes	1	0.03	1.344
15	2	A	4.7 km/s	2	Yes	1	0.01	2.786
16	2	A	4.7 km/s	1	Yes	1	0.5	5.861
17	2	A	4.7 km/s	1	Yes	1	0.3	4.591
18	2	A	4.7 km/s	1	Yes	1	0.1	2.371
19	2	A	4.7 km/s	1	Yes	1	0.05	2.363
20	2	A	4.7 km/s	1	Yes	1	0.01	2.875
21	2	B	4.7 km/s	2	Yes	1	0.9	n/a
22	2	B	4.7 km/s	2	yes	1	0.5	n/a
23	2	B	4.7 km/s	2	Yes	1	0.3	n/a
24	2	B	4.7 km/s	2	Yes	1	0.1	n/a
25	2	B	4.7 km/s	2	Yes	1	0.05	n/a
26	2	B	4.7 km/	2	Yes	1	0.01	n/a
27	2	B	4.7 km/s	1	Yes	1	0.5	1.391
28	2	B	4.7 km/s	1	Yes	1	0.3	1.391
29	2	B	4.7 km/	1	Yes	1	0.1	1.391
30	2	C	4.7 km/s	1	Yes	1	0.05	1.243
31	2	C	4.7 km/s	1	Yes	1	0.03	0.978
32	2	C	4.7 km/s	1	Yes	1	0.01	1.243
33	2	C	4.7 km/s	1	Yes	1	0.05	1.243
34	2	C	4.7 km/s	1	Yes	1	0.01	1.304
35	1	A	Glmpse2plate	None	0.2	Smthco+rough	.	n/a

36	1	A	4.7 km/s	2	0.5	n/a	0.5	1.644
37	1	A	4.7 km/s	2	0.3	n/a	0.3	1.571
38	1	A	4.7 km/s	2	0.2	n/a	0.2	1.441
39	1	A	4.7 km/s	2	0.1	n/a	0.1	1.168
40	1	A	4.7 km/s	2	0.05	n/a	0.05	0.981
41	1	A	4.7 km/s	None	0.5	None	0.5	1.663
42	1	A	4.7 km/s	none	0.3	None	0.3	1.489
43	1	A	4.7 km/s	None	0.2	None	0.2	1.505
44	1	A	4.7 km/s	None	0.1	None	0.1	1.571
45	1	A	4.7 km/s	None	0.05	None	0.05	1.721
46	1	B	4.7 km/s	1	0.9	1	0.9	0.645
47	1	B	4.7 km/s	1	0.5	1	0.5	0.7
48	1	B	4.7 km/s	1	0.3	1	0.3	0.718
49	1	B	4.7 km/s	1	0.2	1	0.2	0.686
50	1	B	4.7 km/s	1	0.1	1	0.1	0.632
51	1	B	4.7 km/s	1	0.05	1	0.05	0.818
52	1	B	4.7 km/s	1	0.01	1	0.01	0.882
53	1	C	4.7 km/s	1	0.9	1	0.9	0.625
54	1	C	4.7 km/s	1	0.5	1	0.5	0.7
55	1	C	4.7 km/s	1	0.3	1	0.3	0.718
56	1	C	4.7 km/s	1	0.2	1	0.2	0.686
57	1	C	4.7 km/s	1	0.1	1	0.1	0.631
58	1	C	4.7 km/s	1	0.05	1	0.05	0.618
59	1	C	4.7 km/s	1	0.01	1	0.01	0.882
60	1	D	4.7 km/s	1	0.5	1	0.5	1.468
61	1	D	4.7 km/s	1	0.3	1	0.3	1.212
62	1	D	4.7 km/s	1	0.1	1	0.1	0.817
63	1	D	4.7 km/s	1	0.05	1	0.05	0.871
64	1	A	Forced lower LVZ	None	yes	None	0.2	
65	2	A	Forced lower LVZ	1	yes	1	0.1	
66	2	D	4.7 km/s	2	Yes	1	1.5	2.612
67	2	D	4.7 km/s	2	Yes	1	1.1	2.612
68	2	D	4.7 km/s	2	Yes	1	0.9	2.612
69	2	D	4.7 km/s	2	Yes	1	0.5	1.508
70	2	D	4.7 km/s	2	Yes	1	0.3	2.612
71	2	D	4.7 km/s	2	Yes	1	0.1	2.612
72	2	D	4.7 km/s	2	Yes	1	0.05	1.34

73	2	D	4.7 km/s	2	Yes	1	0.03	1.344
74	2	D	4.7 km/s	2	Yes	1	0.01	2.786
75	2	D	4.7 km/s	1	Yes	1	1.5	2.629
76	2	D	4.7 km/s	1	Yes	1	1.1	2.62
77	2	D	4.7 km/s	1	Yes	1	0.9	2.617
78	2	D	4.7 km/s	1	Yes	1	0.5	2.436
79	2	D	4.7 km/s	1	Yes	1	0.3	2.014
80	2	D	4.7 km/s	1	Yes	1	0.1	1.182
81	2	D	4.7 km/s	1	Yes	1	0.05	0.951
82	2	D	4.7 km/s	1	Yes	1	0.03	1.007
83	2	D	4.7 km/s	1	Yes	1	0.01	1.053
84	3	D	4.7 km/s	1	Yes	1	0.2	0.758
85	3	D	4.7 km/s	1	Yes	1	0.15	0.767
86	3	D	4.7 km/s	1	Yes	1	0.1	0.774
87	3	D	4.7 km/s	1	Yes	1	0.07	0.779
88	3	D	4.7 km/s	1	Yes	1	0.05	0.78
89	3	D	4.7 km/s	1	Yes	1	0.01	0.784
90	2	D	LVZ forced	1	Yes	1	0.5	n/a
91	2	D	LVZ forced	1	Yes	1	0.1	n/a
92	2	D	LVZ forced	1	Yes	1	0.03	n/a
93	2	D	4.8 all	2	yes	1	0.1	n/a
94	2	D	4.6 all	2	Yes	1	0.1	n/a
95	2	D	4.5 all	2	Yes	1	0.1	n/a
96	1	A	LVZ forced	1	Yes	1	0.9	n/a
97	1	A	LVZ forced	1	Yes	1	0.2	n/a
98	1	A	LVZ forced	1	Yes	1	0.05	n/a

Appendix D. Oceanic Lithosphere Reference Plot

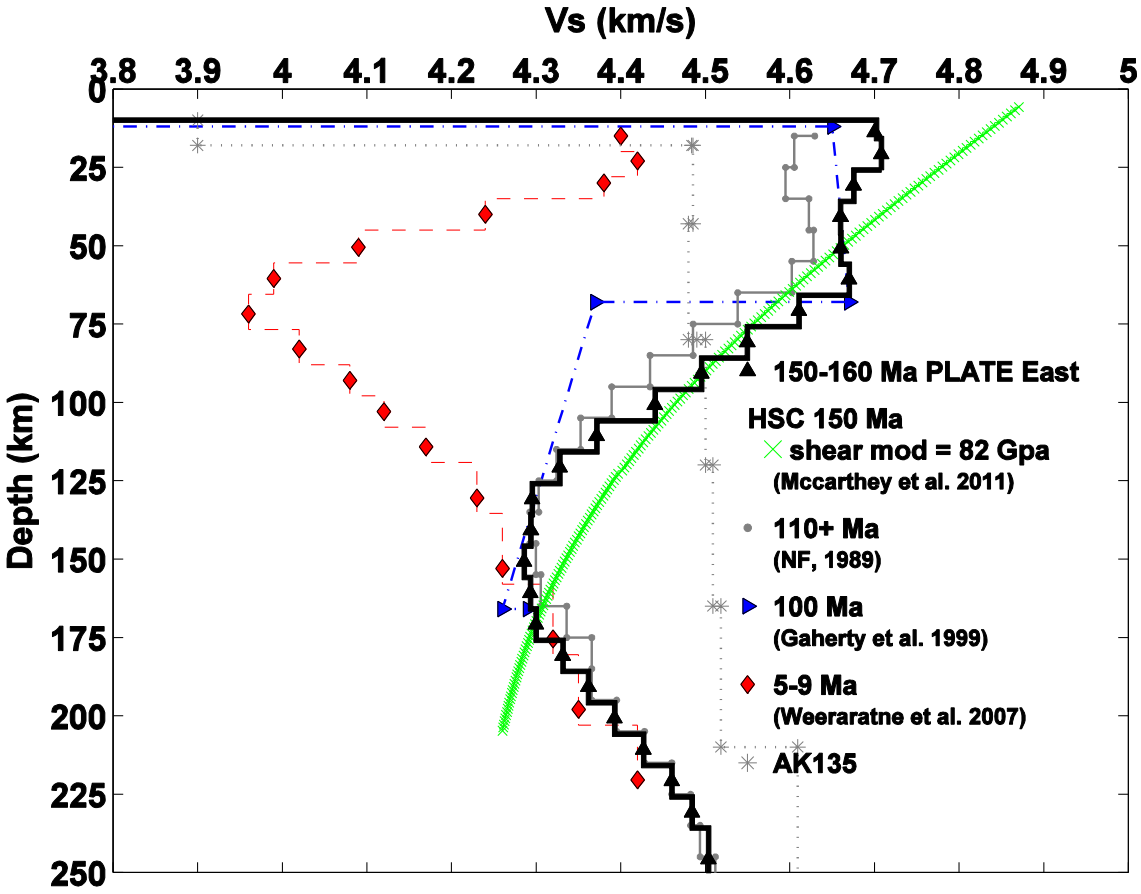

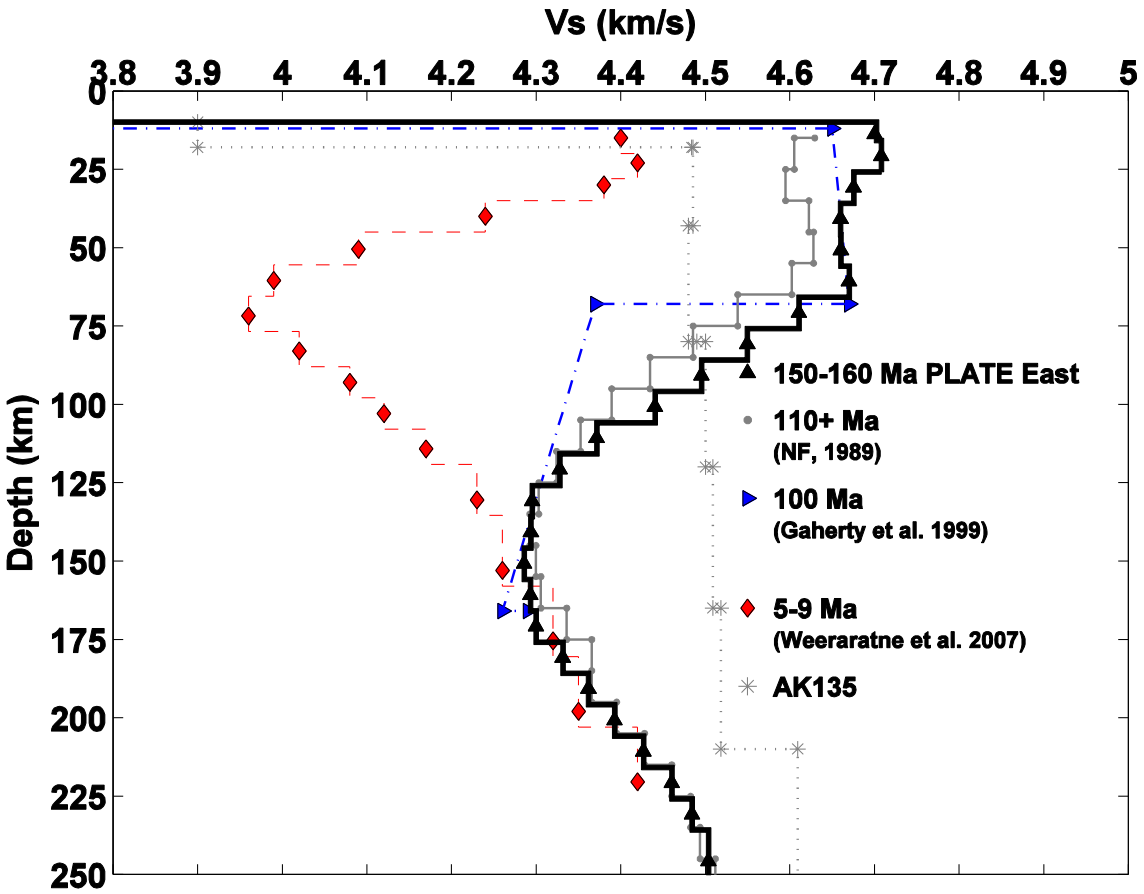
Vs (km/s)
3.8
3.9
4
4.1
4.2
4.3
4.4
4.5
4.6
4.7
4.8
4.9
5
Depth (km)
0
25
50
75
100
125
150
175
200
225
250
150-160 Ma PLATE East
110+ Ma
(NF, 1989)
100 Ma
(Gaherty et al. 1999)
5-9 Ma
(Weeraratne et al. 2007)
AK135

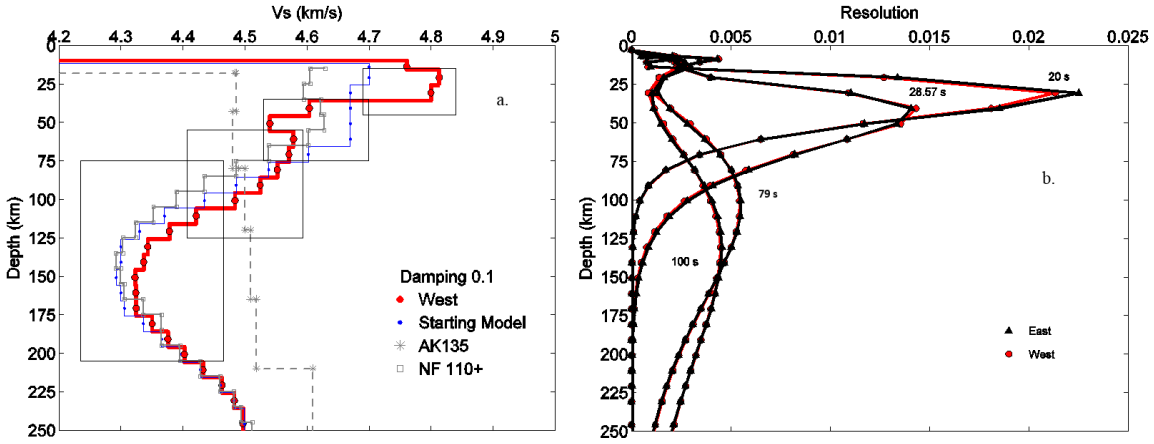
Vs (km/s)
Depth (km)
a.
Damping 0.1
West
Starting Model
AK135
NF 110+
Resolution
20 s
28.57 s
79 s
100 s
b.
East
West

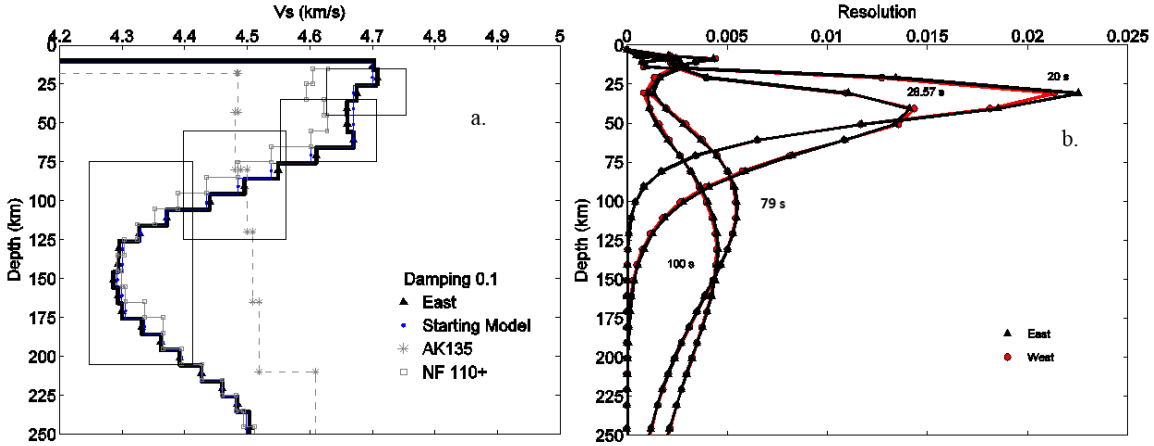
Vs (km/s)
Depth (km)
a.
Damping 0.1
East
Starting Model
AK135
NF 110+
Resolution
20 s
28.57 s
79 s
100 s
b.
East
West

Appendix E. Half Space Cooling Proof

The half-space cooling model for conductive cooling is parameterized by

$$T = T_1 \text{ at } t = 0, y>0 \quad (1a)$$

$$T = T_0 \text{ at } y = 0, t>0 \quad (1b)$$

$$T \to T_0 \text{ at } y = 0, t>0. \quad (1c)$$

This method is a manipulation of multiple similarity ratios to solve for the temperature structure at different isotherms. First we introduce a similarity variable, Θ, which is a dimensionless temperature ratio

$$\theta = \frac{T - T_1}{T_0 - T}. \quad (2)$$

Θ is now used to transform the heat flow equation to

$$\frac{\delta\theta}{\delta t} = \kappa\frac{\delta^2\theta}{\delta y^2} \quad (3)$$

Length parameters are y, which describes the plate thickness, and the diffusion distance which is a length scale $\sqrt{\kappa t}$. Therefore we assume that Θ is a function of the dimensionless ratio

$$\eta = \frac{y}{2\sqrt{\kappa t}}. \quad (4)$$

The problem revolves around the concept of using scaling ot constrain the parameters based on the rank of the problem. The Θ and η introduced are the resulting scaling factors for this problem. We will find that the thermal diffusion length is the distance over which the effects of a sudden, localized change in temperature is felt over time t.

Finding the solution requires the isolation of η for comparison to temperature. This is first done by applying the partial derivatives of Θ with respect to t and y in terms of η

$$\frac{\delta\theta}{\delta t} = \frac{\delta\theta}{\delta n}\frac{\delta n}{\delta t} \tag{5}$$

Plugging in our values with respect to η, the solution yields

$$\frac{\delta\theta}{\delta t} = \frac{\delta\theta}{\delta n}(-\frac{1}{4}\frac{y}{\sqrt{\kappa t}}\frac{1}{t}) = \frac{\delta\theta}{\delta\eta}(-\frac{1}{2}\frac{\eta}{t}). \tag{6}$$

for t and

$$\frac{\delta\theta}{\delta y} = \frac{\delta\theta}{\delta\eta}\frac{\delta\eta}{\delta y} = \frac{\delta\theta}{\delta\eta}(\frac{1}{2\sqrt{\kappa t}}). \tag{7}$$

for y. Since we are trying to restructure equation (3), we want to find the partial derivative of Θ as a second derivative by taking the derivative of equation (7) with respect to y

$$\frac{\delta^2\theta}{\delta y^2} = \frac{\delta^2\theta}{\delta\eta^2}\frac{\delta^2\eta}{\delta y^2}. \tag{8}$$

$$\frac{\delta^2\theta}{\delta y^2} = \frac{\delta^2\theta}{\delta\eta^2}(\frac{1}{2\sqrt{\kappa t}}) = \frac{\delta^2\theta}{\delta\eta^2}(\frac{1}{4\kappa t}). \tag{9}$$

Next, we plug or results from equations (6) and (9) into (3) and simplify:

$$\frac{\delta\theta}{\delta\eta}(-\frac{1}{2}\frac{\eta}{t}) = \kappa(\frac{1}{4\kappa t}\frac{\delta^2\theta}{\delta\eta^2}) \tag{10}$$

$$-\frac{1}{2t}\eta\frac{\delta\theta}{\delta\eta} = \frac{1}{4t}\frac{\delta^2\theta}{\delta\eta^2} \tag{11}$$

$$-\eta\frac{\delta\theta}{\delta\eta} = \frac{1}{2}\frac{\delta^2\theta}{\delta\eta^2}. \tag{12}$$

Now let $\phi = \frac{\delta\Theta}{\delta\eta}$ and substitute it into equation (12)

$$-\eta\phi = \frac{1}{2}\frac{\delta\phi}{\delta\eta} \tag{13}$$

$$\eta\delta\eta = \frac{1}{2}\frac{\delta\phi}{\phi}. \tag{14}$$

Since we have separated the variables, next we integrate both sides of an infinite half-space in order to solve for Θ

$$\int_o^\infty \eta \mathrm{d}\eta = \int_0^\infty \frac{1}{2}\frac{1}{\phi}\,\mathrm{d}\phi \tag{15}$$

$$-\frac{1}{2}\eta^2 = ln(\phi) - ln(c). \tag{16}$$

Since ln(c) is constant, take the inverse of both sides to find

$$\mathrm{e}^{-\frac{1}{2}\eta^2} = \mathrm{e}^{ln(\phi)} - \mathrm{e}^{ln(c)} \tag{17}$$

$$c\mathrm{e}^{-\frac{1}{2}\eta^2} = \phi \ = \frac{\delta\theta}{\delta\eta} \tag{18}$$

Next, we integrate again to solve for Θ

$$\int_0^\infty c\mathrm{e}^{-\eta^2} = \int_0^\infty \frac{\delta\theta}{\delta\eta} \longrightarrow \int_0^\infty c\mathrm{e}^{-\eta^2}\mathrm{d}x = \int_0^\infty \mathrm{d}\theta \tag{19}$$

$$c\int_0^\infty \mathrm{e}^{-\eta^2} = \theta. \tag{20}$$

Since $\frac{\theta}{c} = \frac{\sqrt{\pi}}{2}$, we can extrapolate c through this method

$$\int_0^\infty c\mathrm{e}^{-\eta^2} = \frac{\sqrt{\pi}}{2}. \tag{21}$$

Therefore, c = $\frac{-2}{\sqrt{\pi}}$ and reinserting this gives

$$\theta = 1 - \frac{-2}{\sqrt{\pi}} \int_0^{\eta} \mathrm{e}^{-\eta^2} \mathrm{d}\eta. \tag{22}$$

Utilizing the error function,

$$erf(\eta) = \frac{-2}{\sqrt{\pi}} \int_0^{\eta} \mathrm{e}^{-\eta^2} \mathrm{d}\eta', \tag{23}$$

We can reevaluate Θ based on this property such that

$$\theta = 1 - erf(\eta) = erfc(\eta). \tag{24}$$

Using this property and the definition of the error function, the solution yields

$$\theta = \frac{-2}{\sqrt{\pi}} \int_0^{\eta} \mathrm{e}^{-\eta^2} \mathrm{d}\eta' \tag{25}$$

$$\theta = 1 - erf(\eta) \tag{26}$$

Inserting the values of Θ and its complete indicates

$$\theta = erfc(\eta) \tag{27}$$

$$\frac{T - T_1}{T_0 - T} = erfc\frac{y}{2\sqrt{\kappa t}} \tag{28}$$

Now we can manipulate the equation to solve it in terms of the erf instead of erfc,

$$\frac{T - T_1}{T_0 - T} = 1 - \frac{T - T_0}{T_1 - T_0} = 1 - erf(\eta) = \tag{29}$$

$$\frac{T - T_0}{T_1 - T_0} = erf(\eta). \tag{30}$$

Appendix F. Shearsaito Program

```
c This inversion uses matrix inversion routines from
c Don Forsyth and Aibing Li, simannerr42.f

c This inversion uses phase velocity data for each period
c from surface wave inversion output (e.g. simannerr1.a.f)

c Partial derivatives are simultaneously calculated(output) by s_saito.f
c for dc/dbeta, dc/dalpha, dc/drho and used in this inversion
c for the partial derivative matrix, G,  (just read in).

c Residuals for this inversion are obtained by calculating
c a third set of  phase velocities by running the
c new shear wave velocities and their corresponding P velocities
c (a layered model) through s_saito.f and comparing the
c difference in these phase velocities from the data.

c Fix alpha or
c calculate the new layered model (for residuals) by:
c dalpha=dbeta*sqrt(3) and
c alphanew = alphastart + dalpha
c (betanew is calculated in this inversion similarly)

c Sequential iterations must recalculate a new starting model
c (can use the one used for residuals) from shear wave velocity
c output of this inversion and use it's phase velocities
c as model input. Then invert here for another shear wave profile.
c Use the same phase velocity data (output from simannerr1.a.f)
c (Again, new residuals are calculated as above)
c Also use new partial deriv's from s_saito.f

c Program has now been modified to do any number of iterations
c desired. Still must copy desired starting model to scalifornia_refer.dat
c before running this. The file copied to scalifornia_refer.dat must be
c the same as startmod and startmod2 in input files.

c Forward model: ph.vel. predictions for an input layered model
c (e.g. ak135 or PREM) obtained from s_saito.f



**********Modify here**********
c nit: number of iteration
c partial devirative of phase velocity with respect to shear velocity
c slightly depends on shear velocity, in other word, this inverse problem
c is linear like, so solution will converge very quickly. (nit = 2)
c nit=1, nit=2 show a little difference (a little bit smaller standard deviation with nit=2)
c nit=2, nit=6 almost no difference

c For linear problem, no iteration is need and inverse result doesn't
c rely on the starting model
```

```
c For nonlinear problem, approximate the problem using linear equations,
c and then solve for a convergent solution based on iteration to satisfy
c the minimum regularization. In this case, the solution does depend on
c the starting model, so an appropriate starting model will be greatly appreciated.

      parameter (npermax=16,maxlay=114,maxgrid=20000,nper2dig=12)
**********************************************************************

      real*4   freq(npermax),damp,depth(maxlay)
      real*4   cmminvmmo(maxlay),tempcov,smooth
      real*4   depmin(maxlay),depmax(maxlay)
      real*4         zero,density
      real*4         xxth,xxdens,xxlong,xxdep
      real*4   depmant(100),densmant(100),almant(100),betmant(100)
      real*4   densrat(100)
      real*4   psait(npermax),phasait(npermax),bandsait(npermax)
      real*4   depsait(npermax),xxd5,betsait(npermax)
      real*4   lat,lon,lontemp, lattemp
c     real*4   veltemp(npermax), stdtemp(npermax)
      real*4   Rough(maxlay,maxlay)
c     real*4   oscil2(maxlay,maxlay),oscil(maxlay,maxlay)
      real*4   penalty(maxlay,maxlay)
      real*4   thick(maxlay),dens(maxlay)
      real*4   sumpredvel(npermax)
      real*4   remlon(maxgrid),remlat(maxgrid)
      real*4   rempred(npermax,maxgrid)

      double precision xxstalpha
      double precision stalpha(maxlay),stbeta(maxlay)
      double precision crrntmodb(maxlay),crrntmoda(maxlay)
      double precision crrntmodr(maxlay)
      double precision ccobs(npermax),stbetak135(maxlay)
      double precision origmod(maxlay),eachrank(maxlay)
      double precision ccobstd(npermax),stddevdata(npermax),ddd
      double precision ccpred(npermax),change(maxlay),correct(maxlay)
      double precision ccpredout(npermax),residout(npermax)
      double precision perd(npermax),xxd1,xxd3,xxp,d(npermax)
      double precision g(npermax,maxlay),gtd(maxlay),gtdcmm(maxlay)
      double precision gtg(maxlay,maxlay),savegtg(maxlay,maxlay)
      double precision gtginv(maxlay,maxlay),stddev(maxlay)
      double precision covinv(maxlay,maxlay),cmm(maxlay,maxlay),ccc
      double precision dataimp(npermax),tempimp(maxlay),resid(npermax)
      double precision tempgtginvgt(maxlay,npermax),xxanom
      double precision fcov(maxlay,maxlay)
      double precision sumsq,sigma2,anom(maxlay)
      double precision dca(maxlay,npermax),dcb(maxlay,npermax)
      double precision dcr(maxlay,npermax)
      double precision resmatx(maxlay,maxlay),tempmatx,resparm,rank

      integer*4 iter,icnt,irow,icol,indx(npermax)
      integer*4 nparam,xxd2,xxd4

      character*70 xxd0,newmodlout,flowmantle,covmatin,covmatout
      character*70 startmod,startmod2,phdata,shvelout,shveloutmat
```

```
      character*70 stmodnext,anomalyout,absvelout,resmatrix
      character*70 phseout(npermax)

      read(*,*) nper
c  nper is number of periods.

      read(*,*) stdmult, damp, smthmu, p2s,nit, rmvnegfac,rho2s,
     1     inpcov,invprd

c  stdmult is term to multiply standard deviations by - formal estimates are often too
c  small.. Multiplier should be large enough that period to period fluctuations or
c  lateral fluctuations are of the order of the assigned standard deviations
c
c  inpcov indicates whether prior covariance matrices are to be used - if gt
c  zero, will expect covariance input from previous run. If > zero, then
c  damp and smthmu will have no effect as damping will be performed by
c  a priori matrix
c
c  invprd indicates whether to invert predictions in second iteration (invprd = 1) to obtain
c  smoother model or to just stop at data inversion
c
c  damp is a priori model std deviation in km/s to use as damping parameter
c  for shear velocities
c
c  smthmu is coefficient for smoothing - minimum curvature Use either 0.0 for no application of
c  minimum curvature or 1.0 for optimum damping
c
c  p2s is ratio to assume for p velocity changes compared to s changes. 0 keeps p velocity fixed
c  1.73 makes changes equivalent to Poisson's ratio of 0.25. 1.0 assumes absolute P changes are
c  equal to S changes, which means that S changes fractionally more (such as for sediments or melt
c  effects).
c
c  nit = number of iterations

c  in this version, input nit means nothing. It iterates once to correct for negative lobes
c  of resolution matrix.

c  rmvnegfac  -  multiplicative factor to control multiples of negative wings
c  predicted from resolution matrix to remove from starting model
c
c  rho2s is ratio to assume for fractional density changes compared to fractional s changes.

c       nit = 2
c            nit = 1
cccc LLB thie values following nper2 may not be needed and have been removed from our input file??
           read(*,*) nper2, depth1, error1,ijk1,ijk2,ijk3,topd,bottomd

c  These are variables controlling the search for phase velocity (roots to equations) for
c  given structure. nper2= # periods, depth1 default depth extent, error1, criterion for
c  ending search, ijk1 = 4 is Rayleigh spherical earth, 3 is Love spherical earth, ijk2 = 0, ijk3 = 2
c  topd and bottomd control depth range in which partial derivatives are output
      nobs = nper

      read(*,*) startmod
```

```
            read(*,*) flowmantle
            read(*,*) phdata
            read(*,*) newmodlout
            read(*,*) shvelout
        read(*,*) shveloutmat
        read(*,*) resmatrix
            read(*,*) covmatin
            read(*,*) covmatout

            open(10, file=startmod)
            open(90, file = newmodlout)
            open(52, file = "resolutmtx.d")


cnonode read(10,*) beglat,endlat,dlat,beglon,endlon,dlon
cnonode write(90,*) beglat,endlat,dlat,beglon,endlon,dlon

cnonode nlat = (endlat-beglat)/dlat +1.01
cnonode nlon = (endlon-beglon)/dlon + 1.01
cnonode nxy = nlat*nlon
c  TESTING ONLY, limit nxy
c       nxy = 2

cnonode do i = 1,nper
cnonode   read(*,*) phseout(i)
cnonode   open(60+i, file = phseout(i))
cnonode   write(60+i,*) beglat,endlat,dlat,beglon,endlon,dlon
cnonode enddo

            open(12, file = phdata)

            open(18, file = shvelout)
        open(19, file = shveloutmat)

        open(40, file = flowmantle)

            open(50, file = covmatout)

        open(55, file = "gtginvmtx.d")

CCC!!!!DSW Let's make inpcov = 0. for 1st iteration.
CCC!!! Script will loop back and make one for second loop.
            if (inpcov.gt.0) open(51, file = covmatin)


            read(40,*) nlowlay
        do i=1,nlowlay
              read(40,*) depmant(i),densmant(i),almant(i),betmant(i)
c           write(*,*) depmant(i),densmant(i),almant(i),betmant(i)
            enddo

            close(40)
```

```
c  read in parameters that control interval in which Saito routines search for
c  phase velocity solutions
        open(41, file = 'perstart_plate_don.d')
              do i=1,nper
                read(41,*) psait(i),phasait(i),bandsait(i),betsait(i),depsait(i)
              enddo
              close(41)

        open(52,  file = resmatrix)

              sumnormmsft2 = 0.0
              do i = 1, nper
                sumpredvel(i) = 0.0
              enddo

        write(*,*) 'beginning of loop 1, line 241-ish'
c %%%%%%%%%%%%%%%%%%%%%%%%%%%%%%%%%%%%%%% LOOP 1
%%%%%%%%%%%%%%%%%%%%%%%%%%%%%%%%%%%%%%%%%%%%%%%%%%%%%%
ccc!!!DSW Should nxy just be 1 if I'm NOT incrementing over a million points ? Or comment out this loop
?
ccc!!! BIG LOOP 1 (inxy is one node in a map region of interest)
cnonode do inxy = 1, nxy

cnonode              read(12,*) lon, lat
cnonode          write(*,*) inxy, lon,lat
cnonode          remlon(inxy) = lon
cnonode              remlat(inxy) = lat

c  read in starting shear wave velocity model
c       model to bottomd as starting model
c unit=10: startmod.dat

cnonode  read(10,*) lontemp, lattemp
         read(10,*) nlay

cnonode  write(90,*) lontemp,lattemp
cnonode         write(90,*) nlay
c nlayall: 2X layers, including low mantle parts
c np=nlay: number of layers in the lithosphere and upper mantle
c nparam: number of layers which model needs to be resolved
c shear velocity can be resolved by data
        np = nlay
        nparam = np

ccc!!!DSW below loop is not needed if no apriori covariance matrix is used (inpcov = 0.) cnonode
cnonode if (inpcov.gt.0) then
cnonode   do i = 1,np
cnonode     read(51,*) dummy
cnonode     do j=1,i
cnonode       read(51,*) ii,jj, covinv(i,j)
cnonode       covinv(j,i) = covinv(i,j)
cnonode     enddo
cnonode   enddo
cnonode endif
```

```
*********************************Modify here**************************
c 54 is twice the number of layers in the lower mantle
c       nlayall= 2*np + 54
cLLB     nlayall = 2*nlay + nlowlay
**************************************************************************

ccc!!!DSW Hard Wired file - same as "startab.dat" in DSW old scripts
ccc!!! Here do we need to input "startab.dat" ?
ccc!!! If so - why is it re-writing another one below ?
ccc!!! Lexine thinks it's basically copying "startab.dat" to a new file name (below)
ccc!!!     so we don't have to write over startab.dat every time.


c   first time writing startab, compiles from upperod & lowmanntle
              open(30, file = 'startab.dat')

        zero = 0.
c             write(30,*)'    0    0    0'
        write(30,*)
        write(30,*) '   1'
        write(30,*)'df              col # = 47'
        write(30,*) ' 114    6371.0                  982.0
     r0 0 1'
c         write(30,*) nlayall, '    6371.0                  982.0
        write(30,*)'(4F8.0)'
        do ii=1,np
          read(10,*) thick(ii),dens(ii),stalpha(ii),stbeta(ii)
c  guard against thin water layers that are difficult to compute response for
               if (thick(ii).le.0.4) thick(ii) = 0.401
          write(30,210) zero,dens(ii),stalpha(ii),stbeta(ii)
          write(30,210) thick(ii),dens(ii),stalpha(ii),stbeta(ii)
c               write(*,*) 'stbeta ',ii,stbeta(ii)
c  change sensitivity to shear velocity change to density units
               if (stbeta(ii).ne.0.0) then
                 densrat(ii) = rho2s*dens(ii)/stbeta(ii)
               else
                 densrat(ii) = 0.0
               endif
        enddo


c mantle starting model (below our study depth)
            do i=1,10
          write(30,210) depmant(i),densmant(i),almant(i),betmant(i)
            enddo

       do i=11,nlowlay
          write(30,211) depmant(i),densmant(i),almant(i),betmant(i)
            enddo

211    format (1x,f5.2,2x,f6.4,2x,f7.4,1x,f6.4)
210    format (1x,f5.2,2x,f6.4,2x,f6.4,2x,f6.4)
```

```
            write(30,*) '   4   2872.3'
            write(30,*) '   1'

            write(30,*) '  16  700.0    1.00E-06  4 0 2   0.0        400.0'
c           write(30,310) nper2, depth1, error1,ijk1,ijk2,ijk3,topd,bottomd
            write(30,*) ' (6F10.6,2I2)'
c ***************************************************************************

            do i=1,nper2dig
              write(30,220) psait(i),phasait(i),bandsait(i),betsait(i),
     1       depsait(i)
            enddo

          do i=(nper2dig+1),nper
            write(30,230) psait(i),phasait(i),bandsait(i),betsait(i),
     1       depsait(i)
          enddo

           close(30)
c            stop1
          write(*,*) 'beginning of loop 2, line 337-ish'
C %%%%%%%%%%%%%%%%%%%%%%%%%%%%%%%%%%%%%% LOOP 2
%%%%%%%%%%%%%%%%%%%%%%%%%%%%%%%%%%%%%%%%%%%%%%%%%%%%%%%%%%%%%%%%%%%%%%%
c start loop for iterations (DSW's ORIGINAL BIG LOOP) LOOP 2
           do kk=1,nit

              write(*,*) 'iteration', kk, 'line 354'

cccc first iteration
            if (kk.eq.1) then

             do i=1,np
               origmod(i)=stbeta(i)
               crrntmodb(i)=stbeta(i)
                        crrntmoda(i) = stalpha(i)
                        crrntmodr(i) = dens(i)

c    writing out current mod
c                       write(*,*) 'crrntmodb,crrntmoda',crrntmodb(i),crrntmoda(i)
             enddo

            endif

            if (kk.eq.1) then
c read in observed data
                 do i=1,nobs
                   read(12,*) ccobs(i),ccobstd(i)
c multiply standard deviations by constant to compensate for usual underestimate
!
                   stddevdata(i)=stdmult*ccobstd(i)
                 enddo
```

```
**********modify here**************************
c set up apriori damping of model parameters

c covinv(i,i) for minimum length damping only (uses diagonals of Cmm only)
c for non zero's only on the diagonals, matrix inverse is easy:
c inverse = 1/damp**2 on individual diagonals
       if (inpcov.eq.0) then
            do i=1,np
              do j = 1,np
                covinv(i,j) = 0.0
              enddo
              covinv(i,i)=1./(damp**2)
            enddo

c######### Don's new stuff
c--------------------------------
ccc!!!?? Question 4 Don: We were looking at shearz16.f - at the new section that designates a "Rough
Matrix". Does the number 1,-4,6,-3 mean something physical unique to a study ccc!!!?? area - or are these
just smoothing choices that can be applied to all studies ?

c       write(*,*) 'Dons smoothing stuff, line 379'

c Rough matrix
      do irow = 1, np
      do icol = 1, np
         Rough(irow,icol) = 0.0
       enddo
      enddo
c---------------------------------
c                          !------ this definition of smoothness
       Rough(2,1) = -3         !------ matrix has minimum first order
       Rough(2,2) = 6          !------ derivative constraint on edges
       Rough(2,3) = -4         !
       Rough(2,4) = 1          !
       Rough(np-1,np-3) = 1     !
       Rough(np-1,np-2) = -4    !
       Rough(np-1,np-1) = 6     !
       Rough(np-1,np) = -3      !
c--------------------------------


      do irow = 3, np-2
        icol = irow
        Rough(irow, icol-2) = 1
        Rough(irow, icol-1) = -4
        Rough(irow, icol) = 6
        Rough(irow, icol+1) = -4
        Rough(irow, icol+2) = 1
      enddo

c-------------------------------------------------------------!
c fix the water and sediment layers (by heavy damping)       !
              do i = 1,np                                    !
```

```
          if(stbeta(i).lt.1.5) then                    !
            Rough(i,i) = 1.0E+4
                covinv(i,i) = 1.0E+4                        !
          endif                                    !
              enddo                                  !
c-------------------------------------------------------------!
        endif
                                                          !
       endif      !-----------------------------------kk-----------------------------!

c*************************************************************************



       if (kk.gt.1) then

c            write(*,*) 'iteration 2, line 424'
c%%%%%% HARD WIRED file name
        open(30, file = 'startab.dat')

c             write(30,*)'    0    0    0'
        write(30,*)
        write(30,*) '   1'
        write(30,*)'df              col # = 47'
c         write(30,*)' 130    6371.0                  982.0
c     r     0 0 1'
        write(30,*) ' 114    6371.0                  982.0
    r0 0 1'
        write(30,*)'(4F8.0)'
        do ii=1,np
          write(30,210) zero,crrntmodr(ii),crrntmoda(ii),crrntmodb(ii)
          write(30,210) thick(ii),crrntmodr(ii),crrntmoda(ii),
    1             crrntmodb(ii)
c               write(*,*)'crrntmodb',ii, crrntmoda(ii),crrntmodb(ii)
        enddo

c        write(*,*) 'line 450'
c mantle starting model (below our study depth)
           do i=1,10
          write(30,210) depmant(i),densmant(i),almant(i),betmant(i)
           enddo

       do i=11,nlowlay
          write(30,211) depmant(i),densmant(i),almant(i),betmant(i)
           enddo

           write(30,*) '   4   2872.3  0'
           write(30,*) '   1'

           write(30,*) '  16  700.0    1.00E-06  4 0 2   0.0        400.0'
c          write(30,310) nper2, depth1, error1,ijk1,ijk2,ijk3,topd,bottomd
           write(30,*) ' (6F10.6,2I2)'
```

```
c       write(*,*) 'line 462'

       do i=1,nper2dig
            write(30,220) psait(i),phasait(i),bandsait(i),betsait(i),
     1      depsait(i)
            enddo

       do i=(nper2dig+1),nper
            write(30,230) psait(i),phasait(i),bandsait(i),betsait(i),
     1      depsait(i)
            enddo

        close(30)
       endif
c LLB end of iterations routine
c *********************************************************************
c        write(*,*) 'line 478, calling s_saito again'
c calculate predicted phase velocities from s_saito.f

        call s_saito

c            write(*,*) 'after calling s_saito again, line 483'

c  initialize g matrix
       do irow = 1, nobs
       do icol = 1, np
         g(irow,icol) = 0.0
       enddo
       enddo

c  data vector and partial derivatives listed event by event with all
c  real data for first event followed by imaginary data, then onto next event
c  d contains misfit to starting model

c data vector is difference of observed and predicted phase velocities
c del d in inversion equation
c use apriori stdev?
c      stop 3
            open(16, file='DERIV.DATA')
            do i=1,nobs

c read in predicted data
c here c(w) obtained from s_saito which also calculates
c partial derivatives,dcb,dca
c from a starting layered model (e.g. ak135 or PREM)
c for Rayleigh waves dcb=combo of P and SV:
c e.g., dcb(z)=dcb + p2s*dca

          read(16,*) xxd0                    !!!!unit=16:  DERIV.DATA
          read(16,*) xxd1
          read(16,*) xxd2,xxd3,perd(i),ccpred(i)
          read(16,*) xxd4
```

```
c          write(*,*)'pred,ccpred',perd(i),ccpred(i)
               do j=1,np
                read(16,*) depth(j),dcr(j,i),dca(j,i),dcb(j,i)
c  assume P velocity changes are proportional to shear velocity with ratio p2s
           g(i,j)= ((dcb(j,i) + p2s*dca(j,i)+densrat(j)*dcr(j,i))
     r          *thick(j))/stddevdata(i)
                enddo
              enddo


         close (16)
              write(18,*) 'residuals of starting model'
              write(18,*) 'obs        pred        resid    norm resid'
410      format(4F9.4)
              sumstartres = 0.0
       do i=1,nobs
               d(i)=(ccobs(i)-ccpred(i))/stddevdata(i)
               write(18,410) ccobs(i),ccpred(i),ccobs(i)-ccpred(i), d(i)
               sumstartres = sumstartres + d(i)**2
       enddo
         sumstartres = sqrt(sumstartres/nobs)
         write(18,*) 'normalized RMS misfit ', sumstartres
c              stop
c  Calculate gtg and gtd
        do j = 1, np
         gtd(j) = 0.0
         do i = 1, nobs
           gtd(j) = gtd(j) + g(i,j)*d(i)
         enddo
          cmminvmmo(j) = 0.0



c  construct gtg
         do jj = 1,j
           gtg(jj,j) = 0.0
           do i = 1, nobs
             gtg(jj,j)= gtg(jj,j) + g(i,jj)*g(i,j)
           enddo
           gtg(j,jj) = gtg(jj,j)
           savegtg(j,jj) = gtg(j,jj)
           savegtg(jj,j) = gtg(jj,j)
         enddo
        enddo

c  Combination of minimum length and curvature
c   add smoothness constraint (minimum curvature). Find coefficient, smthco,
c  that minimizes, in least squares sense, the off-diagonal terms of gtg,
c   which should lead to minimal off-diagonal terms of covariance matrix
c
c%%%%%%%%%%%%%%%%%%%%%%%%%%%%%
ccc!!! DSW Below inpcov stuff is Don's new stuff from old DSW codes
             if (inpcov.eq.0) then
               sumsmth2 = 0.0
               sumsmgg = 0.0
               do ismth = 2,np
```

```
              do jsmth = 1, ismth-1
                sumsmth2 = sumsmth2 + rough(ismth,jsmth)**2
                sumsmgg = sumsmgg + rough(ismth,jsmth)*
     1                  gtg(ismth,jsmth)
            enddo
              enddo
              smthco = -sumsmgg/sumsmth2
              smthco = smthco*smthmu
           do j = 1,np
            do i = 1,np
              gtg(i,j) = gtg(i,j) +covinv(i,j)+smthco*Rough(i,j)
            enddo
c   add to gtd Tarantola term penalizing misfit to original starting model
c  For one-sided correction, do not penalize changes from original starting model in
c  the iteration
            do i=1,np
              tempcov = (covinv(j,i)+smthco*Rough(j,i))
     1                  *(crrntmodb(i)-origmod(i))
              cmminvmmo(j) = cmminvmmo(j) + tempcov
                enddo
            gtdcmm(j) = gtd(j) - cmminvmmo(j)
           enddo
              else
           do j = 1,np
            do i = 1,np
              gtg(i,j) = gtg(i,j) +covinv(i,j)
            enddo
            gtdcmm(j) = gtd(j) - cmminvmmo(j)
           enddo
              endif


c  Invert gtg. gtg will be destroyed.
C  Not the most efficient approach because doesn't take advantage of
c  symmetry of gtg. Use LU decomposition from Press et al.
         do i= 1,np
           do j = 1, np
             gtginv(i,j)= 0.0D0
           enddo
             gtginv(i,i) =1.0D0
         enddo

         call dludcmp(gtg,maxlay,np,nparam,indx,ddd)
         do j = 1,np
         call dlubksb(gtg,maxlay,np,nparam,indx,gtginv(1,j))
         enddo


c  Find change to starting model
         do i= 1, np
           change(i)=0.0
           do j = 1,np
             change(i) =change(i) + gtdcmm(j)*gtginv(i,j)
           enddo
```

```
c               write(*,*) 'change',change(i)
        enddo
c  Find rank (sum of diagonals of resolution matrix), i.e., number of
c  pieces of information or number of independent model parameters

        rank = 0.0

            do i=1,np
          resparm =0.0
          do j = 1,np
            resparm = resparm + gtginv(i,j)*savegtg(j,i)
          enddo
                eachrank(i) = resparm
            rank = rank + resparm
        enddo

c calculate entire resolution matrix
c can plot rows of resmatx with depth and see resolution kernals
            do k = 1,np
              do i = 1,np
                tempmatx = 0.0
                do j = 1,np
                      tempmatx = tempmatx + gtginv(k,j)*savegtg(j,i)
                enddo
                resmatx(k,i) = tempmatx
              enddo
            enddo

c write resmatrix
            if (kk.eq.nit) then
ccc DSW %%%%% DO we need thiw write lon,lat below ?
cnonode        write(52,*) lon, lat
            do i=1,np
              do j=1,np
              write(52,*) resmatx(i,j)
c write out gtginv matrix for beta errors in depth layers
           write(55,*) gtginv(i,j)
              enddo
        enddo
            endif
 152    format(i2,1x,25f6.3)
c Find data importances, diagonals of g*gtginv*gt
c g*gtginv*gt : data resolution matrix

            do j=1,np
              do i=1,nobs
                      tempimp(i) = 0.0
                      do k=1,np
                        tempimp(i) = tempimp(i) + gtginv(j,k)*g(i,k)
                      enddo
                      tempgtginvgt(j,i) = tempimp(i)
              enddo
            enddo
```

```
            do i=1,nobs
              dataimp(i)=0.0
              do j=1,np
                dataimp(i) = dataimp(i) + g(i,j)*tempgtginvgt(j,i)
              enddo
            enddo


c  Update current model  - check for absurd results of low shear velocity
c         write(*,*) 'updating current model'
          do ii = 1, np
           crrntmodb(ii) = crrntmodb(ii) + change(ii)
                if ((ii.gt.1).and.(crrntmodb(ii).lt.1.0)) crrntmodb(ii) = 1.0
c               write(*,*)'crrntmodb + change',crrntmodb(ii),change(ii)
          enddo
c  Check to make sure shear velocity in water layer stays at zero
          if (abs(origmod(1)).lt.0.1) crrntmodb(1) = 0.0
          do j = 1, np
           stddev(j) = sqrt(gtginv(j,j))
          enddo

c calculate new layered earth model for input to saito.f to get
c residuals for this inversion
c write out velocities in saito.f format

c         write(*,*) 'writing startab again, line 707'

            zero = 0.00


          open(30,file = 'startab.dat')
c               write(30,*) '    0    0    0'
          write(30,*)
          write(30,*) '   1'
          write(30,*)'df              col # = 47'
c         write(30,*)' 130    6371.0                 982.0
c     r     0 0 1'
          write(30,*) ' 114    6371.0                 982.0
     r0 0 1'

          write(30,*)'(4F8.0)'

            do ii=1,np
              crrntmoda(ii) = crrntmoda(ii) + p2s*change(ii)
              crrntmodr(ii) = crrntmodr(ii) + densrat(ii)*change(ii)
              write(30,210) zero,crrntmodr(ii),crrntmoda(ii),crrntmodb(ii)
              write(30,210) thick(ii),crrntmodr(ii),crrntmoda(ii),
     r           crrntmodb(ii)
c             write(*,*)'crrntmodb',ii,crrntmodb(ii)
            enddo

            do i=1,10
           write(30,210) depmant(i),densmant(i),almant(i),betmant(i)
```

```
            enddo

       do i=11,nlowlay
         write(30,211) depmant(i),densmant(i),almant(i),betmant(i)
            enddo

            write(30,*) '   4   2872.3'
            write(30,*) '   1'

c**********************************Modify
here*****************************************
c  18 is number of periods and 210 is the maximum depth where the data can constrain
            write(30,*) '  16  700.0    1.00E-06  4 0 2   0.0        400.0'
c           write(30,310) nper2, depth1, error1,ijk1,ijk2,ijk3,topd,bottomd
c310     format(I5,F7.1,E12.2,1x,3I2,F6.1,F12.1)
c*******************************************************************************************
**
            write(30,*) ' (6F10.6,2I2)'

       do i=1,nper2dig
             write(30,220) psait(i),phasait(i),bandsait(i),betsait(i),
    1       depsait(i)
            enddo

            do i=(nper2dig+1),nper
              write(30,230) psait(i),phasait(i),bandsait(i),betsait(i),
    r     depsait(i)
            enddo

220   format (4x,f6.3,5x,f5.3,5x,f5.3,5x,f5.3,4x,f7.3)

230   format (3x,f7.3,5x,f5.3,5x,f5.3,5x,f5.3,3x,f8.3)

        close(30)
c       stop 2
c         write(*,*) 'line 765'

              write(18,*) 'damp, smthmu, rank', damp, smthmu, rank
              write(18,*)'depth  beta   stddev  abschange change  each rank'

            do ii = 1, np
         write(18,180)depth(ii), crrntmodb(ii), stddev(ii),
    r         (crrntmodb(ii)-origmod(ii)), change(ii), eachrank(ii)

       enddo

180    format(F6.2,5F8.4)

            write(18,*) 'data importance'
            do i=1,nobs
              write(18,*) i,real(dataimp(i))
            enddo
```

```
c calculate residuals for the new shear wave vel. profile
c must calculate new phase velocities from saito.f with this
c beta(z) profile and get difference from data

ccccccccccccllb7/27
       close(unit = 16)

c       write(*,*) 'about to call s_saito 3, line 791'

           call s_saito

c       write(*,*) 'calling s_saito 3, line 793'
c      stop
     open(16, file = 'DERIV.DATA')

            write(18,*)'T       obs        pred       data stddv       residuals
    1    norm residuals'
       sumresid  = 0.0
      do i=1,nobs
         read(16,*) xxd0
         read(16,*) xxd1
         read(16,*) xxd2,xxd3,xxp,ccpredout(i)
c              write (*,*) "iter ", i,xxp,ccpredout(i)
         read(16,*) xxd4
c          write(*,*)'line 815'
              residout(i) = ccobs(i) - ccpredout(i)

         write(18,190)perd(i),ccobs(i),ccpredout(i),stddevdata(i),
    &          residout(i),residout(i)/stddevdata(i)


         sumresid = sumresid + (residout(i)/stddevdata(i))**2
              do j=1,np
                    read(16,*) xxd5
              enddo
c        write(*,*)'line826'
           enddo
              RMS = sqrt(sumresid/nobs)
         standardresid = sqrt(sumresid/(nobs-rank))  !!!!nobs-rank is degree of freedom of models
              if (kk.eq.nit) sumnormmsft2 = sumnormmsft2 + standardresid**2
              write(18,*)
              write(18,*) '   RMS    stddv(divided by degree of freedom)'     !!!! for model
              write(18,*) RMS,  standardresid
              write(18,*)
190     format(F6.2, 2F12.4, 3F14.4)

     close(unit = 16)
c  Correct for effect of negative lobes in resolution matrix
c   only happens during first nit
c        if (kk.lt.nit) then
c             do i = 1, np
c               correct(i) = 0.0
c             enddo
```

```
c              do j = 1, np
c                do j = 1,np
c  make this correction one-sided - correct only if deeper
c  i.e. effect of change in layer j on deeper layers is corrected
c            do i = j,np
c                 if (resmatx(i,j).lt.0.0) then
c                   correct(i) = correct(i) +
c     r            resmatx(i,j)*change(j)/resmatx(j,j)
c                 endif
c               enddo
c              enddo
c              do i = 1,np
c                write(18,*) i, correct(i)
cCCC RUN#1: ignores all corrections below except density (2nd iteration)
c               crrntmodb(i) = crrntmodb(i) - correct(i)
c               crrntmoda(i) = crrntmoda(i)- p2s*correct(i)
c  Try correcting from starting model
CCC RUN#2: uses correction below - contrained to stbeta(i) (1st iteration)
CCC RUN#3: uses correction below - contrained to stbeta(i) (2nd iteration)
c               crrntmodb(i) = stbeta(i) - rmvnegfac*correct(i)
c               crrntmoda(i) = stalpha(i)- rmvnegfac*p2s*correct(i)
c               crrntmodr(i) = dens(i) - rmvnegfac*densrat(i)*correct(i)
c            write(19,*) depth(i), crrntmodb(i), stddev(i), eachrank(i)
c           enddo
c             endif

       if (kk.eq.nit) then
         do ii = 1,np
           write(19,*)depth(ii), crrntmodb(ii), stddev(ii), eachrank(ii)
         enddo
       endif

      close(unit = 19)
c %%%%%%%%%%%%%%%%%%%% CLOSE the second BIG LOOP 2 (DSW original)
%%%%%%%%%%%%%%%%%%%%%%%%%%%%%%%%%%%%%%%%%%%%%%%%%%%%%%%%%%%%%%%%
      enddo  ! close loop from iterations
cccc LLB do we need this loop, just writes to unused file.
             do ii = 1, np

c%%%%%%%%%%%%%% WRITE out depth here and plot depth and velocities from THIS file
%%%%%%
c          write(90,290) depth(ii),crrntmodr(ii),crrntmoda(ii),
c     r      crrntmodb(ii)
               write(90,*) depth(ii),crrntmodr(ii),crrntmoda(ii),
     r      crrntmodb(ii)
c%%%%%%%%%%%%%% KNOW WHAT you're plotting. Are you plotting here or above ?
ccc!!!           write(19,*)depth(ii), crrntmodb(ii), stddev(ii), eachrank(ii)
             enddo
290     format (f6.3,2x,f5.3,2x,f6.3,2x,f6.3)

c %%% NO NODES, NEED THIS line below ?
cnonode        write (50,*) inxy

ccccc Write out the gtginv matrix for beta errors in depth layers
```

```
      do i = 1,np
            do j= 1,i
              write(50,*) i,j,gtginv(i,j)
            enddo
          enddo

c           do i = 1, nper
c             write(60+i,*) lon,lat,velsum1(i),velsum2(i)
c             write(60+i,*) lon,lat,ccpredout(i)
c             sumpredvel(i) = sumpredvel(i) + ccpredout(i)
c           enddo

ccc What ? Why is this summing phvels over all periods for one node ?
cnonode       do i = 1, nper
cnonode   rempred(i,inxy) = ccpredout(i)
cnonode   sumpredvel(i) = sumpredvel(i) + ccpredout(i)
cnonode enddo

c %%%%%%%%%%%%%%%%%%%%%%%%%%%%%%%%%%%%%%%%%%%%%%%%%%%%%%%% CLOSE the
first BIG LOOP 1 %%%%%%%%%%%%%%%%%%%%%%%%%%%%%%%%%%%%%%%%%%%%
cnonode enddo  ! close all grid points

ccc!!!DSW HOW MUCH of this stuff below matters ?

ccc!!! measure of misfit averaged over all nodes - LEXINE doesn't need this junk below.
cnonode avgnormmsft2 = sumnormmsft2/nxy
cnonode write(50,*) avgnormmsft2, ' avgnormmsft2'
cnonode write(18,*) avgnormmsft2, ' avgnormmsft2'

cc!!! DSW do we need these averages below ? Maybe not ?
cnonode do i = 1, nper
cnonode         avgvel = sumpredvel(i)/nxy
cnonode   write(60+i,*) avgvel
cnonode   do inxy = 1, nxy
cnonode     write(60+i,*) remlon(inxy), remlat(inxy), rempred(i,inxy)
cnonode   enddo

ccc!!! LEXINE figure out if you ever open 60+i anywhere above ?
cnonode   close(60+i)  !?? Do we eliminate this too ?

cnonode enddo

      write(*,*) 'we finished!'

           close(10)
      close(unit = 12)
      close(18)
           close(50)
           close(51)
      close(52)
           close(90)
    stop
    end
```

```
      SUBROUTINE dlubksb(a,maxlay,n,np,indx,b)
      INTEGER n,np,indx(n)
      DOUBLE PRECISION a(maxlay,maxlay),b(n)
      INTEGER i,ii,j,ll
      DOUBLE PRECISION sum
      ii=0
      do 12 i=1,n
        ll=indx(i)
        sum=b(ll)
        b(ll)=b(i)
        if (ii.ne.0)then
          do 11 j=ii,i-1
            sum=sum-a(i,j)*b(j)
11        continue
        else if (sum.ne.0.) then
          ii=i
        endif
        b(i)=sum
12      continue
      do 14 i=n,1,-1
        sum=b(i)
        do 13 j=i+1,n
          sum=sum-a(i,j)*b(j)
13        continue
        b(i)=sum/a(i,i)
14      continue
      return
      END


      SUBROUTINE dludcmp(a,maxlay,n,np,indx,d)
      INTEGER n,np,indx(n),NMAX
      double precision d,a(maxlay,maxlay),TINY
      PARAMETER (NMAX=500,TINY=1.0e-20)
      INTEGER i,imax,j,k
      double precision aamax,dum,sum,vv(NMAX)
      d=1.
      do 12 i=1,n
        aamax=0.
        do 11 j=1,n
          if (abs(a(i,j)).gt.aamax) aamax=abs(a(i,j))
11        continue
        if (aamax.eq.0.) write(*,*) 'singular matrix in ludcmp'
        vv(i)=1./aamax
12      continue
      do 19 j=1,n
        do 14 i=1,j-1
          sum=a(i,j)
          do 13 k=1,i-1
            sum=sum-a(i,k)*a(k,j)
13        continue
          a(i,j)=sum
14        continue
```

```
      aamax=0.
      do 16 i=j,n
        sum=a(i,j)
        do 15 k=1,j-1
          sum=sum-a(i,k)*a(k,j)
15      continue
        a(i,j)=sum
        dum=vv(i)*abs(sum)
        if (dum.ge.aamax) then
          imax=i
          aamax=dum
        endif
16      continue
      if (j.ne.imax)then
        do 17 k=1,n
          dum=a(imax,k)
          a(imax,k)=a(j,k)
          a(j,k)=dum
17      continue
        d=-d
        vv(imax)=vv(j)
      endif
      indx(j)=imax
      if(a(j,j).eq.0.)a(j,j)=TINY
      if(j.ne.n)then
        dum=1./a(j,j)
        do 18 i=j+1,n
          a(i,j)=a(i,j)*dum
18      continue
      endif
19    continue
    return
    END
```